ELECTRONIC STRUCTURE IN THE ORGANIC-BASED MAGNET $[Fe^{II}(TCNE)(NCMe)_2][Fe^{III}Cl_4]$ USING THE ORTHOGONALIZED LINEAR COMBINATION OF ATOMIC ORBITALS METHOD WITH HUBBARD U

A THESIS IN
Physics

Presented to the Faculty of the University
of Missouri-Kansas City in partial fulfilment of
the requirements for the degree

MASTER OF SCIENCE

by
STEVEN CHASE GRAFTON

B.S., University of Missouri, 2006

Kansas City, Missouri
2017

ELECTRONIC STRUCTURE IN THE ORGANIC-BASED MAGNET $[Fe^{II}(TCNE)(NCMe)_2][Fe^{III}Cl_4]$ USING THE ORTHOGONALIZED LINEAR COMBINATION OF ATOMIC ORBITALS METHOD WITH HUBBARD U

Steven Chase Grafton, Candidate for the Master of Science Degree

University of Missouri-Kansas City, 2017

ABSTRACT

The Hubbard U parameter is applied to the organic-based magnet $[Fe^{II}(TCNE)(NCMe)_2][Fe^{III}Cl_4]$ using the Orthogonalized Linear Combination of Atomic Orbitals (OCLAO) methods. The Local Spin Density Approximation (LSDA) method plus the Hubbard U parameter is used to account for on-site atomic Coulombic repulsion and exchange correlation interactions for the *d* orbitals of the Fe^{II} atoms. Applying the Hubbard U parameter results in an increased band gap and clear spin splitting.

APPROVAL PAGE

The Faculty listed below, appointed by the Dean of the College of Arts and Sciences, have examined a thesis titled "Electronic Structure in the Organic-based Magnet $[Fe^{II}(TCNE)(NCMe)_2][Fe^{III}Cl_4]$ using the Orthogonalized Linear Combination of Atomic Orbitals Method with Hubbard U", presented by Steven Chase Grafton, candidate for the Master of Science degree, and certify that in their opinion, it is worthy of acceptance.

Supervisory Committee

Paul Rulis, Ph.D., Committee Chair
Department of Physics and Astronomy

Wai-Yim Ching, Ph.D.
Department of Physics and Astronomy

Elizabeth Stoddard, Ph.D.
Department of Physics and Astronomy

TABLE OF CONTENTS

LIST OF ILLUSTRATIONS

Figure Page

LIST OF TABLES

ACKNOWLEDGEMENTS

I would like to thank Professor Paul Rulis, my advisor. His guidance, time, and inexhaustible patience were critical for completing this work.

Thank you to my parents who gave me every opportunity to learn and explore my interest in science.

To my wife, Melissa, thank you for your unfailing support, your love, and, when needed, a kick in the pants.

CHAPTER 1

INTRODUCTION

Context

Current technologies continue to progress in complexity through a self-reinforcing cycle. New technologies necessitate the development of myriad different materials and these materials enable the development of new technologies. A primary bottleneck in the efficient operation of this feedback loop is the fact that the materials often need to optimize a unique or controllable property or combination of properties.[1–5] Unfortunately, this is a costly and laborious activity. First, serious consideration must be given to determine if a given material is *capable* of being optimized to the level(s) required for satisfying application parameters. Then, significant effort must be applied to learn how to tune each of the properties (which are usually not independent and which may sometimes work in opposition to each other). This creates a need for systematic and iterative testing and exploration of the space of synthesis parameters. However, the iterative process of fabrication and testing can potentially be avoided with the advent of computational studies. Computational predictions can save time, money, materials, and resources by simulating the properties of the target material according to the dictates of fundamental physical laws, thereby removing the need to synthesize and test large numbers of samples.[6,7]

A large target area of interest is magnetic materials. Considering inorganic magnetic materials first, we have seen their widespread use across commercial and industrial sectors through digital storage media, power generation in electric motors, routine medical procedures, fundamental scientific investigations, *etc*.[8–11] Traditionally, inorganic magnets have been fabricated through experimental and resource intensive

methods as described above. While numerous breakthrough materials with immense technological applicability have arisen through that approach the effort has been costly.

An interesting alternative to inorganic magnets are organic-based magnets, which are also known as molecule-based magnets or molecular magnets. These materials also have vast application potential because of their combination of inherent magnetism and an organic structure which enables them to be easily synthesized (in principle) through traditional organic chemistry methods. Additionally, they are soluble in a variety of solvents, can be made to produce uniform crystallized structures, are compatible with biological substances, and have the ability to incorporate multiple functional properties such as optical transparency and electrical insulation.[12] Conventional magnets usually contain only metals or metal oxides where only unpaired d- or f-type electrons on the metal ion contribute to the magnetization. In contrast, the organic molecule and coordination complex-based composition of organic-based magnets lead to magnetization from unpaired electrons on the metal ion and/or s and p electrons from the organic species. With respect to the materials optimization process many of the same problems remain. Therefore, there is an even greater need for a computational approach that can model these materials and filter out configurations that are unlikely to be useful while homing in on useful configurations.

Unfortunately, there are a number of challenges associated with performing simulations that model the electronic structure of organic magnets. The presence of interacting unpaired d and f electrons in organic-based magnets are a challenge to current electronic structure calculations. The most popular method of the present day for studying electronic structure, density functional theory (DFT[13,14]), obtains a representation for the

ground state wave function of a given system in terms of non-interacting electrons with the addition of a correction term. The correction term (a functional of the electron density) accounts for so-called exchange and correlation effects (detailed later), but the true form for the functional is not known analytically. Many approximations have been developed, but, when the correlation effect becomes particularly strong these methods tend to perform poorly. When multiple electrons are in the d or f orbitals of a transition metal or rare earth atom the close proximity of the orbital lobes to each other enhances the electron correlation effect. The standard approximations do not account for that repulsive effect and the electrons are allowed to be closer to each other than would otherwise be the case. As a result, many transition metal oxides with d and f electrons are computed to have a band structure showing metallic character when they are, in fact, insulators. Accurately accounting for the interaction of electrons in d and f orbitals in computational studies can offer a significant advantage when predicting material properties for magnetic applications.

Motivation

This thesis will focus on improving the description of the electronic structure and resultant properties of a specific material within the tetracyanoethylene (TCNE) family of organic-based magnet while using the orthogonalized linear combination of atomic orbital (OLCAO) method for calculations conducted. The organic-based magnet of interest is $[Fe^{II}(TCNE)(NCMe)_2][Fe^{III}Cl_4]$ where Me = methyl. Fe-TCNE has a layered magnetic structure with MeCN ligands separating the layers. The Fe^{II} ion bonds to four TCNE anions while two MeCN ligands bond perpendicularly to the Fe^{II} ion. The $Fe^{III}Cl_4$ anion is located between the layers, but has been reported not to contribute to the magnetic ordering (Fig. 1).[15,16] The magnetic behavior orders as a ferrimagnet below a T_c = 90 K and spin

polarization has been experimentally reported.[15,17] A band gap of 40 meV has been previously calculated with an older version of the Orthogonalized Linear Combination of Atomic Orbitals method.

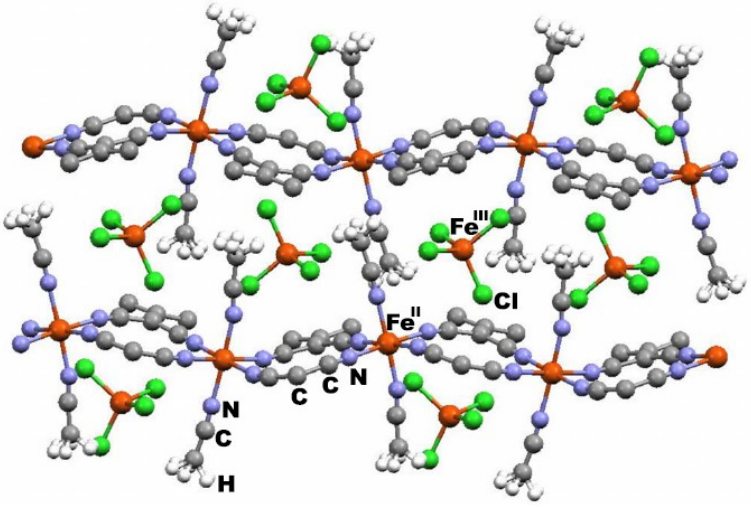

Figure 1. Crystal structure of $[Fe(TCNE)(NCMe)_2][FeCl_4]$ (H, white; C, gray; N, blue; Cl, green; Fe, red). Due to structural disorder each methyl group displays 6 H atoms.[18]

In addition to Fe, the TCNE structure can bond with other metals including V, Mn, Co, and Ni. A number of calculations have been performed for these materials; however, only preliminary investigations for Fe[TCNE] have been performed using OLCAO.

Outline

Chapter Two describes a wide range of fundamental theoretical developments that are needed for understanding the Fe-TCNE calculations. In particular, Hartree-Fock theory and density functional theory are introduced to emphasize the role of exchange and correlation effects in obtaining good electronic band structures. After a description of various exchange and correlation functionals in common use the Hubbard U method is introduced as a direct modification of the exchange-correlation effect that is specific to

strongly correlated electrons that share a common *d*- or *f*- orbital at a given atomic site. Finally, the program code that actually implements the theory is described.

Chapter Three presents the detailed program development activities that were undertaken for this research. The code that the development was built on is the OLCAO method. The OLCAO method is an implementation of many of the theoretical methods described in Chapter Two. Important practical information regarding the implementation is presented here.

Chapter Four presents the results of applying the OLCAO method with the new Hubbard U based exchange-correlation functional to the organic magnet Fe-TCNE. The important data such as spin polarized density of states and symmetric spin-polarized band structure is presented.

In Chapter Five a summary of the Thesis is presented and placed into the context of potential future work, both for exchange-correlation functional development in the OLCAO method and for the development of organic magnets.

CHAPTER 2

THEORETICAL METHODS

Electronic Structure Problem

The goal of most electronic structure theory calculations is to solve the non-relativistic time-independent many-body Schrodinger equation shown in Equation (1).

$$\hat{H}\Psi(\{\mathbf{R}_A\},\{\mathbf{r}_i,\sigma_i\}) = E\Psi(\{\mathbf{R}_A\},\{\mathbf{r}_i,\sigma_i\}) \quad (1)$$

In a system containing M nuclei and N electrons the many-body wavefunction (Ψ) is a function of all nuclear spatial coordinates ($\{\mathbf{R}_A\}$, $A = 1, 2,\ldots, M$) and of all electronic spatial and spin coordinates ($\{\mathbf{r}_i, \sigma_i\}$, $i = 1, 2,\ldots, N$).

The Hamiltonian ($\hat{H}$) is a sum of all possible interactions between nuclei and electrons. The Hamiltonian can be expanded as shown in Equation (2).

$$\begin{aligned}\hat{H} = &-\sum_{i=1}^{N}\frac{\nabla_i^2}{2} - \sum_{A=1}^{M}\frac{\nabla_A^2}{2M_A} \\ &+ \sum_{i=1}^{N}\sum_{j>i}^{N}\frac{1}{|\mathbf{r}_i - \mathbf{r}_j|} \\ &+ \sum_{A=1}^{M}\sum_{B>A}^{M}\frac{Z_A Z_B}{|\mathbf{R}_A - \mathbf{R}_B|} - \sum_{i=1}^{N}\sum_{A=1}^{M}\frac{Z_A}{|\mathbf{r}_i - \mathbf{R}_A|}\end{aligned} \quad (2)$$

For Equation (2) M_A is the ratio of the mass of nucleus A to the mass of an electron and Z_A is the atomic number of nucleus A. The ∇_i^2 and ∇_A^2 are the Laplacian operators for the electrons and nuclei, respectively. The first term represents the kinetic energy of all electrons. The second term represents the kinetic energy of all nuclei. The third term accounts for the Coulomb repulsion between electrons while the fourth term is the

Coulomb repulsion between nuclei. The final term is the Coulomb attraction between electrons and nuclei.

For a many-body quantum system of particles Equation (2) is essentially impossible to solve exactly. The calculations would need to deal with *N*+*NZ* individual particles. Different approximations are needed to reduce this problem to a manageable level.

Born-Oppenheimer Approximation

The first approximation to be made is the Born-Oppenheimer approximation.[19] This approximation uses the fact that the protons and neutrons that make up a nucleus are much heavier than the electrons in a given atom. A proton is roughly 1800 times more massive than an electron. This difference in inertia causes protons to move extremely slowly in response to any combination of motions from the surrounding electrons. Born and Oppenheimer used this fact to consider the nuclei stationary compared to the electrons. The stationary nuclei can be considered classical particles and become an external source of electric potential. This allows the calculations to reduce from *N*+*NZ* individual particles to *NZ* individual particles. The impact of the Born-Oppenheimer approximation to the Hamiltonian of Equation (2) is that select terms change. The second term representing the kinetic energy of the nuclei is now ignored. The fourth term containing the Coulomb repulsion between nuclei now becomes a constant. The resultant equation is called the electronic Hamiltonian and is shown in Equation (3).

$$\widehat{H}_e = -\sum_{i=1}^{N} \frac{\boldsymbol{\nabla}_i^2}{2} + \sum_{i=1}^{N} \sum_{j>i}^{N} \frac{1}{|\mathbf{r}_i - \mathbf{r}_j|} - \sum_{i=1}^{N} \sum_{A=1}^{M} \frac{Z_A}{|\mathbf{r}_i - \mathbf{R}_A|} \tag{3}$$

Using the electronic Hamiltonian, the Schrodinger equation now becomes Equation (4).

$$\widehat{H}_e \Psi_e(\{\mathbf{R}_A\}, \{\mathbf{r}_i, \sigma_i\}) = E_e \Psi_e(\{\mathbf{R}_A\}, \{\mathbf{r}_i, \sigma_i\}) \quad (4)$$

Because the nuclear coordinates, $\{\mathbf{R}_A\}$, are now in a fixed configuration its explicit dependence can be dropped. Additionally, it is common to combine the electronic spatial coordinates and spin coordinates, $\{\mathbf{r}_i, \sigma_i\}$, into one variable $\{\mathbf{x}_i\}$. Equation 4 can be written as Equation (5):

$$\widehat{H}_e \Psi_e(\{\mathbf{x}_i\}) = E_e \Psi_e(\{\mathbf{x}_i\}) \quad (5)$$

Even with the Born-Oppenheimer approximation, solving the interaction between the electrons is extremely difficult because each one interacts with all of the others (an interacting many-body problem) and because the electrons are fermionic quantum mechanical particles that require an anti-symmetric wave function. The many-body interactions are correlated so that predicting the motion of one electron would require knowledge of the instantaneous coordinates of each other electron, meaning that the calculation grows to be a problem of 3^N variables for an *N*-electron system. Notwithstanding this challenging problem many approximation schemes going beyond the Born-Oppenheimer approximation have been devised. Most involve a different representation of the Schrodinger (or Schrodinger-like) equation by converting the *N*-electron Schrodinger equation into an effective one-electron Schrodinger equation. Two overarching schemes will be presented: (1) wave function based methods and (2) density functional based methods. This thesis will primarily concern itself with density functional based methods, so wave function based methods will be described briefly.

Wave Function Based Methods

The fundamental entity of interest for wave function based methods is, of course, the solid state wave function itself. In this approach, an expression for the solid state wave function is directly constructed as a linear combination of products of spin-orbitals with unknown coefficients in such a way so as to satisfy the antisymmetric structure required by electrons. In most cases, the object of interest is further defined to be the ground state wave function. Excited state wave functions tend to be more complicated, but are usually derived from the ground state. The ground state wave function is the wave function with the lowest total energy and it can be obtained through the use of the variational principle, detailed below.

The first step for the determination of the wave function is an educated guess usually influenced by empirical data or past calculations. Next the variational principle dictates that the expectation value of the electronic Hamiltonian ($\widehat{H}_e$) of the trial wave function will always be larger than the true electronic ground state energy, $E_0[\Psi_0]$. The equality, $E[\Psi] \geq E_0[\Psi_0]$, will also hold when the trial wave function is in the true ground state. The use of the variational principle allows one to consider any trial wave function and take incremental steps towards the ground state wave function. The power of the variational principle can now be applied to minimize the approximated wave function.

The Hartree-Fock approximation is the first major development for accurately describing interacting electrons by executing the process described above.[20,21] The Hartree-Fock expression for the wave function, $\Psi(\{\mathbf{x}_i\})$, is compactly represented by a single Slater determinant. The Slater determinant is a linear combination of the product of independent electron wave functions, $\{\phi_i(\mathbf{x}_i)\}$. These independent electron wave functions are also

called spin orbitals. The structure of the Slater determinant inherently satisfies the antisymmetrization requirement mentioned above. Antisymmetry (or inversion of the overall wave function sign with an exchange of the spatial coordinates of two electrons) is a requirement because electrons are fermions that obey Pauli's exclusion principle. The resultant Hartree-Fock wave function for a many-electron system is shown in Equation (6).

$$\Psi(\{\mathbf{x}_i\}) \approx \Psi^{HF}(\{\mathbf{x}_i\}) = \frac{1}{\sqrt{N!}} \begin{vmatrix} \phi_i(\mathbf{x}_i) & \phi_j(\mathbf{x}_i) & \cdots & \phi_N(\mathbf{x}_i) \\ \phi_i(\mathbf{x}_j) & \phi_j(\mathbf{x}_j) & \cdots & \phi_N(\mathbf{x}_j) \\ \vdots & \vdots & \ddots & \vdots \\ \phi_i(\mathbf{x}_N) & \phi_j(\mathbf{x}_N) & \cdots & \phi_N(\mathbf{x}_N) \end{vmatrix} \tag{6}$$

Each of the columns in the Slater determinant is labeled by a spin orbital. Any interchange of columns is reflected in the resulting equation as the swapping of the spatial coordinates of two electrons combined with an overall sign change of the determinant, satisfying again the antisymmetrization requirement. The simplest example to show this process is with the two-electron system in Equations (7-10) where Equation (9) exchanges the columns.

$$\Psi^{HF}(\mathbf{x}_1, \mathbf{x}_2) = \frac{1}{\sqrt{2!}} \begin{vmatrix} \phi_1(\mathbf{x}_1) & \phi_2(\mathbf{x}_1) \\ \phi_1(\mathbf{x}_2) & \phi_2(\mathbf{x}_2) \end{vmatrix} \tag{7}$$

$$\Psi^{HF}(\mathbf{x}_1, \mathbf{x}_2) = \frac{1}{\sqrt{2!}} [\phi_1(\mathbf{x}_1)\phi_2(\mathbf{x}_2) - \phi_2(\mathbf{x}_1)\phi_1(\mathbf{x}_2)] \tag{8}$$

$$\Psi^{HF}(\mathbf{x}_2, \mathbf{x}_1) = \frac{1}{\sqrt{2!}} \begin{vmatrix} \phi_2(\mathbf{x}_1) & \phi_1(\mathbf{x}_1) \\ \phi_2(\mathbf{x}_2) & \phi_1(\mathbf{x}_2) \end{vmatrix} \tag{9}$$

$$\Psi^{HF}(\mathbf{x}_2, \mathbf{x}_1) = \frac{1}{\sqrt{2!}} [\phi_2(\mathbf{x}_1)\phi_1(\mathbf{x}_2) - \phi_1(\mathbf{x}_1)\phi_2(\mathbf{x}_2)] \tag{10}$$

Examining Equations (8) and (10) reveals that the antisymmetry requirement is met as shown in Equation (11).

$$\Psi^{HF}(\mathbf{x}_1, \mathbf{x}_2) = -\Psi^{HF}(\mathbf{x}_2, \mathbf{x}_1) \tag{11}$$

Now that the general Hartree-Fock wave function has been established it can be used to find actual observables. The observable of most interest is the expectation value of the total electronic energy as shown in Equation (12). Starting with Dirac notation:

$$\begin{aligned} E^{HF} &= \langle \Psi^{HF} | \hat{H}_e | \Psi^{HF} \rangle \\ &= \sum_{i=1}^{N} \int \phi_i^*(\mathbf{x}_i) \left[-\frac{\boldsymbol{\nabla}_i^2}{2} + V^{ext}(\mathbf{x}_i) \right] \phi_i(\mathbf{x}_i) d\mathbf{x}_i \\ &+ \frac{1}{2} \sum_{i=1}^{N} \sum_{j=1}^{N} \iint \phi_i^*(\mathbf{x}_i) \phi_j^*(\mathbf{x}_j) \frac{1}{|\mathbf{r}_i - \mathbf{r}_j|} \phi_j(\mathbf{x}_j) \phi_i(\mathbf{x}_i) d\mathbf{x}_i d\mathbf{x}_j \\ &- \frac{1}{2} \sum_{i=1}^{N} \sum_{j=1}^{N} \iint \phi_i^*(\mathbf{x}_i) \phi_j^*(\mathbf{x}_j) \frac{1}{|\mathbf{r}_i - \mathbf{r}_j|} \phi_j(\mathbf{x}_i) \phi_i(\mathbf{x}_j) d\mathbf{x}_i d\mathbf{x}_j \end{aligned} \tag{12}$$

In the above equation V^{ext} is a defined external potential. This equation is interpreted as an energy functional, $E^{HF}[\{\phi_i^*(\mathbf{x}_i)\},\}\phi_i(\mathbf{x}_i)\}]$. Functionals will be expanded on in the next section when density functional based methods are discussed. This energy functional can be variationally minimized using the method of undetermined Lagrange multipliers with the constraint that the set of independent electron wave functions $\{\phi_i(\mathbf{x}_i)\}$ are orthonormal, i.e., $\langle \phi_i(\mathbf{x}_i) | \phi_j(\mathbf{x}_j) \rangle = \delta_{ij}$ where δ_{ij} is the Kronecker delta. Therefore, a mapping from the many-electron Schrodinger equation to effective one-electron Schrodinger-like equations can occur.

$$\hat{F}_i \phi_i(\mathbf{x}_i) = \varepsilon_i \phi_i(\mathbf{x}_i) \tag{13}$$

$$\hat{F}_i = -\frac{\boldsymbol{\nabla}^2}{2} + V^{ext}(\mathbf{x}_i) + V^{Hartree}(\mathbf{x}_i) + V_i^{Exchange}(\mathbf{x}_i) \tag{14}$$

$\hat{F}_i$ is the Fock operator that represents the one-electron Hamiltonian. Eigenvalues and eigenfunctions are represented by ε_i and $\phi_i(\boldsymbol{x}_i)$, respectively. The first term in $\hat{F}_i$ is the

kinetic energy operator for *N*-independent electrons. The second term, V^{ext}, is the external potential which is the Coulomb attraction between the i^{th} electron and all of the nuclei. The third and fourth terms contain approximations for the many-body electron interactions. $V^{Hartree}$ is the Hartree potential; this is the Coulomb repulsion between the i^{th} electron and the electron density from all other electrons.

$$V^{Hartree}(\mathbf{x}_i) = \int \frac{n(\mathbf{x}_j)}{|\mathbf{r}_i - \mathbf{r}_j|} d\mathbf{x}_j \tag{15}$$

$$n(\mathbf{x}_j) = \sum_{j=1}^{N} |\phi_j(\mathbf{x}_j)|^2 \tag{16}$$

It is important to note that the electron density from all other electrons is an averaged density. That is, the potential due to other electrons is derived from their average spatial distribution and not their instantaneous position. Proceeding from the Coulombic repulsion between individual electrons to the repulsion between averaged densities is a significant approximation. The unaccounted energy difference between those two Coulombic repulsion expressions is one of the biggest disadvantages of Hartree-Fock theory. Density functional methods, discussed later, are a powerful way to overcome this failure.

The fourth term, called the exchange potential, $V_i^{Exchange}$, is necessary in order to account for the antisymmetry of the wave function. This term is a consequence of quantum mechanics and does not have a classical analogue. The form of $V_i^{Exchange}$ is shown in Equation (17).

$$V_i^{Exchange}(\mathbf{x}_i) = \sum_{j=1}^{N} \int \phi_j^*(\mathbf{x}_j) \frac{1}{|\mathbf{r}_i - \mathbf{r}_j|} \phi_j(\mathbf{x}_i) d\mathbf{x}_j \tag{17}$$

As mentioned above, the use of an average electron density, also called an effective mean field, in Hartree-Fock theory leads to an incomplete description of the spatial charge distribution. The missing item is identified as electron correlation. In fact, the difference between an exact ground state electronic energy and the approximated ground state Hartree-Fock electronic energy is named the correlation energy.[22] Even though this can be a small contribution to the overall energy, it is significant enough to influence physical and chemical properties of interest.

There are many quantum chemistry-based methods that are designed to go beyond Hartree-Fock[23] theory by including correlation effects. Some widely used methods include configuration interaction, Møller-Plesset perturbation theory, and coupled cluster theory. These will be described very briefly. Configuration interaction[24] is a variational method that uses a linear combination of Slater determinants for its wave function. The 'configuration' refers to the electron configuration represented in each of the Slater determinants (e.g. one electron excitation, two electron excitation, etc.) and the 'interaction' refers to those different configurations or states interacting according to the same variational principle as were originally used for one Slater determinant. Because the number of possible configurations grows factorially this method usually requires excessive amounts of computational time (even when the series is truncated) and is therefore limited in practical application to small, typically molecular, systems. Møller-Plesset[25] is, as indicated by the name, a perturbation theory that uses Rayleigh-Schrodinger perturbation theory. Like any perturbation theory, Møller-Plesset starts with a simple model and if the perturbations are not too large, then the desired observables can be obtained. The coupled cluster technique makes use of an exponential cluster operator in its wave function,

Equation (18). In Equation (19) this operator T is a summation of T_n operators that account for excited states whether they be occupied or virtual (unoccupied). This method has been employed for small to medium-sized systems.[26,27]

$$\Psi_{cc} = e^{T}\phi_0 = (1 + T + \frac{1}{2!}T^2 + \frac{1}{3!}T^3 + \cdots)\phi_0 \tag{18}$$

$$T = T_1 + T_2 + T_3 + \cdots + T_n \tag{19}$$

Density Functional Theory

The principal difference between density functional theory and the wavefunction based methods described above is the use of the electron density $n(\mathbf{r})$ as the item of interest. Density functional theory has become the most widely used approach for electronic structure calculations today, especially in condensed matter physics, because of the combination of its economical computational requirements and its largely acceptable accuracy. The higher performance derives from the fact that the electron density $n(\mathbf{r})$ is one variable of three dimensions while wavefunction based methods require construction of an explicit expression for all N electrons, each with its own three spatial dimensions. Because the work in this thesis contains an extension of the density functional theory formalism a more detailed discussion of density functional theory will be presented than the previous section regarding wavefunction based methods. Many articles and textbooks have been written reviewing density functional theory. A selection of these is referenced in the bibliography.[28–33]

The electron density is defined for normalized wave functions as (Equation (20))

$$n(\mathbf{r}) = N \int \cdots \int |\Psi(\mathbf{x}_1, \mathbf{x}_2, \ldots, \mathbf{x}_N)|^2 \, d\mathbf{x}_1 d\mathbf{x}_2 \cdots d\mathbf{x}_N \tag{20}$$

where $\{\mathbf{x}_i\} = \{\mathbf{r}_i, \sigma_i\}$ represents the spatial and spin coordinates of the electrons. Equation (20) determines the probability of finding any of the *N* electrons within a volume located at *r* with arbitrary spin. The electron density can also be integrated to yield the total number of electrons in the system (Equation 21).

$$N = \int n(\mathbf{r}) d\mathbf{r} \tag{21}$$

Thomas-Fermi Model

The first density-based approach to the electronic structure of solids was the Thomas-Fermi model. In the 1920s Llewellyn Thomas and Enrico Fermi developed a semi-classical theory applying the electronic density to determine the electronic energy.[34,35] This is considered an important precursor to modern density functional theory because it achieves the goal of using the electron density as the sole input to ascertain the electron energy. The quantum statistics of a uniform or homogeneous electron gas are used to derive the electronic kinetic energy. The electron-nucleus and electron-electron interactions are treated classically. Thus, the kinetic energy of the electrons in this model is defined as (Equation 23)

$$T[n] = C_F \int [n(\mathbf{r})]^{5/3} \, d\mathbf{r} \tag{22}$$

where

$$C_F = \frac{3}{10}(2\pi^2)^{2/3} = 2.871 \tag{23}$$

In this approach an approximation is made to the kinetic energy that depends solely on the electron density. Adding the electron-nucleus and electron-electron interaction energies to the electronic kinetic energy, the total energy is found as (Equation 24).

$$E[n] = C_F \int [n(\mathbf{r})]^{5/3}\, d\mathbf{r} - Z \int \frac{n(\mathbf{r})}{r}\, d\mathbf{r} + \frac{1}{2} \int \int \frac{n(\mathbf{r}_1) n(\mathbf{r}_2)}{|\mathbf{r}_1 - \mathbf{r}_2|}\, d\mathbf{r}_1 d\mathbf{r}_2 \qquad (24)$$

The semi-classical Thomas-Fermi model will not provide highly accurate ground state energies. The impact of the model is that it shows that the energy can be obtained by using the electron density.

Functionals

Before we begin to review modern density functional theory, the concept and properties of functionals must be introduced. In general, a functional $F[n]$ is a function that takes a vector as its argument and returns a scalar, similar to how a function $y = f(x)$ takes a scalar *x* and returns a scalar *y*. A pertinent example of a functional is the particle number or the electron number from Equation (22).

$$N = \int n(\mathbf{r}) d\mathbf{r} = N[n] \qquad (25)$$

This is a rule for obtaining the number *N* given the function $n(\mathbf{r})$ as its input. A property of functionals to note is that it does not matter what the argument of *n* is since the functional only depends on the function itself and not the variable of the function. For example, it is not necessary to distinguish between $F[n(\mathbf{r})]$ and $F[n(\mathbf{r}')]$.

A function $y = f(x)$ can be varied in two ways: the argument *x* can be varied or *f* can be varied. For the function $f(x)$ the ordinary differential *dy* measures how *y* changes when the variable *x* becomes $x \to x + dx$. This is the everyday ordinary calculus with which most people are familiar. In a similar fashion, the functional variation δy measures how the value of y changes as a result of the variation of the function $f(x)$. This is the calculus of variations.

Derivatives of functionals can be obtained in a similar way as ordinary derivatives. In an ordinary derivative df/dx measures the change of $y = f(x)$ when changing *x*. This is the familiar slope of $f(x)$ (Equation 26).

$$f(x + dx) = f(x) + \frac{df}{dx}dx + O(dx^2) \tag{26}$$

Expanding this idea to functionals, a functional derivative measures the change in the functional when the function of its argument changes (Equation 27).

$$F[f(x) + \delta f(x)] = F[f(x)] + \int s(x)\delta f(x)dx + O(\delta f^2) \tag{27}$$

The integral is required because the function *f* is varied over all points. The functional slope, or $s(x)$ coefficient, is defined as the functional derivative (Equation 28).

$$s(x) = \frac{\delta F[f]}{\delta f(x)} \tag{28}$$

A general form for a function $n(x)$ of functional $F[n]$ is (Equation 29)

$$F[n] = \int f(n, n', n'', n''', \dots; x)dx \tag{29}$$

Here the primes denote ordinary derivatives of the function $n(x)$ with respect to *x*. The functional derivative can be written as (Equation 30).[32]

$$\frac{\delta F[n]}{\delta n(x)} = \frac{\partial f}{\partial n} - \frac{d}{dx}\frac{\partial f}{\partial n'} + \frac{d^2}{dx^2}\frac{\partial f}{\partial n''} - \frac{d^3}{dx^3}\frac{\partial f}{\partial n'''} + \cdots \tag{30}$$

This expression is used with considerable frequency in modern density functional theory to obtain exchange-correlation potentials from exchange-correlation energies. These topics will be further discussed in later sections.

Hohenberg-Kohn Theorems

Modern density functional theory was formally solidified with the theorems of Pierre Hohenberg and Walter Kohn in 1964.[13] These theorems express the electronic Hamiltonian as a functional of $n(\mathbf{r})$ and are summarized here.

i. There exists a one-to-one correspondence between the external potential $v(\mathbf{r})$ and the electron density $n(\mathbf{r})$.

ii. The ground state electron density can be found using the variational principle.

Typically, one first considers the positions of the atomic nuclei and then anticipates that the electron density will be dependent on the external potential that it produces. That is, the external potential $v(\mathbf{r})$ of the electronic Hamiltonian depends explicitly on the nuclear configuration. However, working from the electron density first, theorem (i) states that one can invert the usual line of thinking and obtain $v(\mathbf{r})$ from $n(\mathbf{r})$ to within an additive constant. Thus, crucially, the entire electronic Hamiltonian can be expressed as a functional of $n(\mathbf{r})$. The derivations are reviewed here.

Consider a non-degenerate system where there is a collection of electrons enclosed in a box. There is an external potential $v(\mathbf{r})$ acting on the system. Assume the electron density is known and that it determines the $v(\mathbf{r})$ and the associated properties. If there exists a different external potential $v'(\mathbf{r})$ that differs from $v(\mathbf{r})$ by more than an additive constant that can also produce the same ground state electron density $n(\mathbf{r})$, then there are two different Hamiltonians, $\widehat{H}$ and $\widehat{H}'$. The ground state electron density of these two Hamiltonians would be the same, but the normalized wave functions Ψ_0 and Ψ_0' would be different. Expressing the above mathematically (Equation 31).

$$
\begin{aligned}
E_0 &< \langle \Psi_0' | \widehat{H} | \Psi_0' \rangle \\
&< \langle \Psi_0' | H' + V - V' | \Psi_0' \rangle \\
&< \langle \Psi_0' | H' | \Psi_0' \rangle + \langle \Psi_0' | V - V' | \Psi_0' \rangle \\
&< E_0' + \int n_0'(\mathbf{r}) \, [v(\mathbf{r}) - v'(\mathbf{r})] d\mathbf{r}
\end{aligned}
\tag{31}
$$

Where E_0 and E_0' are the ground state energies for $\widehat{H}$ and $\widehat{H}'$ Hamiltonians, respectively. The last step has used the result that

$$
\langle \Psi_0' | V | \Psi_0' \rangle = \int n_0'(\mathbf{r}) v(\mathbf{r}) d\mathbf{r} \tag{32}
$$

This comes from the definition

$$
n_0'(\mathbf{r}) = \int |\Psi(\mathbf{r}, \mathbf{r}_2 \ldots \mathbf{r}_N)|^2 \, d\mathbf{r} \ldots d\mathbf{r}_N \tag{33}
$$

Similarly, (Equation 34)

$$
\begin{aligned}
E_0' &< \langle \Psi_0 | \widehat{H}' | \Psi_0 \rangle \\
&< \langle \Psi_0 | H + V' - V | \Psi_0 \rangle \\
&< \langle \Psi_0 | H | \Psi_0 \rangle + \langle \Psi_0 | V' - V | \Psi_0 \rangle \\
&< E_0 + \int n_0(\mathbf{r}) [v'(\mathbf{r}) - v(\mathbf{r})] d\mathbf{r}
\end{aligned}
\tag{34}
$$

If it is then assumed that the different ground state wavefunctions can produce the same ground state density, then $n_0(\mathbf{r}) = n_0'(\mathbf{r})$. Adding Equation (31) and Equation (34) one can obtain Equation (35).

$$
E_0 + E_0' < E_0' + E_0 \tag{35}
$$

This is an obvious contradiction. Therefore, no two potentials that are different by more than a constant can produce the same electronic density $n(\mathbf{r})$. Further, $n(\mathbf{r})$ uniquely determines $v(\mathbf{r})$ (with the associated ground state properties).

Given an external potential $v(\mathbf{r})$ the energy E_v can be written explicitly as a function of the electron density $n(\mathbf{r})$ (Equation 36).

$$\begin{aligned} E_v[n] &= T[n] + V_{ne}[n] + V_{ee}[n] \\ &= \int n(\mathbf{r})v(\mathbf{r})d\mathbf{r} + F_{HK}[n] \end{aligned} \tag{36}$$

Where

$$F_{HK}[n] = T[n] + V_{ee}[n] \tag{37}$$

In Equation 36 V_{ne} and V_{ee} are the nucleus-electron and electron-electron interaction energies, respectively. Note that $F_{HK}[n]$ ('*HK*' denotes '*Hohenberg-Kohn*') is only dependent on $n(\mathbf{r})$ and is independent from any external potential $v(\mathbf{r})$, so $F_{HK}[n]$ is a universal functional of $n(\mathbf{r})$. The first HK theorem has freed us to produce an expression for the ground state energy that is not directly derived from a solid-state wave function and which instead comes from the electron density. Thus, if we can guess the correct electron density, then we can obtain the ground state energy.

The second Hohenberg-Kohn theorem states that the electronic density that minimizes the ground state total energy will be the exact ground state electronic density (Equation 38),

$$E_0[n_0] \leq E_v[n] \tag{38}$$

and that the ground state energy can be obtained using the variational principle. Consider the ground state wave function Ψ with its related electron density $n(\mathbf{r})$. From the first theorem we have that $n(\mathbf{r})$ uniquely determines the external potential $v(\mathbf{r})$. If there is another wave function Ψ' with electron density $n'(\mathbf{r})$, then one has Equation (39).

$$\langle \Psi' | \hat{H} | \Psi' \rangle = \int n'(\mathbf{r})v(\mathbf{r})d\mathbf{r} + F_{HK}[n'] = E[n'] \geq E[n] \tag{39}$$

Consequently, the total energy will reach a minimum only when the electron density is the ground state electron density.

If $F_{HK}[n]$ was a known and relatively simple function of $n(\mathbf{r})$, then solving for the ground state energy and density for a given external potential would be a straightforward exercise since it only requires the minimization of a functional of a three-dimensional density function. Unfortunately, the functional is not simple. Therefore, a key part of the study of many-electron systems is the determination of the universal functional $F_{HK}[n]$.

Kohn-Sham Equations

In 1965 Walter Kohn and Lu Jeu Sham presented equations that turned density functional theory into a tool for practical electronic structure calculations.[14] Because the Thomas-Fermi model is a semi-classical model it does not appropriately describe the kinetic energy of the interactions. To resolve this, Kohn and Sham re-introduced the concept of *non-interacting* electrons moving in an effective field. That is, the kinetic energy was broken into two terms, one that contained the kinetic energy of non-interacting electrons at the given density and a second term that contained the residual, unknown, contribution to the kinetic energy due to the true interacting nature of the electrons. The functional $F_{HK}[n(\mathbf{r})]$ is then expressed as a sum of the kinetic energy of non-interacting electrons, T_s, the Hartree energy, $E^{Hartree}$, and the remaining many-body and quantum effects (e.g. interacting part of the kinetic energy and exchange). These terms are consolidated into E_{xc}, the exchange and correlation energy (Equation 40).

$$E[n] = \int n(\mathbf{r})v(\mathbf{r})d\mathbf{r} + F_{HK}[n(\mathbf{r})]$$
$$= \int n(\mathbf{r})v(\mathbf{r})d\mathbf{r} + T_s\,[n(\mathbf{r})] + E^{Hartree}[n(\mathbf{r})] + E_{xc}[n(\mathbf{r})] \tag{40}$$

Defining the effective potential (Equation 41)

$$V^{eff} = \frac{\delta\{\int n(\mathbf{r})v(\mathbf{r})d\mathbf{r} + E^{Hartree}[n(\mathbf{r})] + E_{xc}[n(\mathbf{r})]\}}{\delta n(\mathbf{r})}$$
$$= v(\mathbf{r}) + \int \frac{n(\mathbf{r}')}{|\mathbf{r} - \mathbf{r}'|}d\mathbf{r}' + v_{xc}(\mathbf{r}) \tag{41}$$

where $v_{xc}(\mathbf{r})$ is the exchange-correlation potential defined as (Equation 42)

$$v_{xc}(\mathbf{r}) = \frac{\delta E_{xc}[n(\mathbf{r})]}{\delta n(\mathbf{r})} \tag{42}$$

Equation (41) gives us the opportunity to write a central equation in the Kohn-Sham formulation of density functional theory. This is the one-electron Schrodinger-like equation (Equation 43).

$$\left[-\frac{1}{2}\nabla^2 + V^{eff}\right]\phi_i = \epsilon_i\phi_i \tag{43}$$

The set of one-electron Kohn-Sham orbitals, $\{\phi_i\}$, are not formally related to any physical atomic orbitals or electronic energy levels, but they can be used formally to obtain both the total energy and the electron density (Equation 44).

$$n(\mathbf{r}) = \sum_{i=1}^{N} |\phi_i|^2 \tag{44}$$

Clearly, the ϵ_i's are the energy eigenvalues of the Kohn-Sham one-electron orbitals. The total energy is determined from the density in (Equation 45)

$$E = \sum_{i=1}^{N} \epsilon_i - \frac{1}{2}\int\int \frac{n(\mathbf{r})n(\mathbf{r}')}{|\mathbf{r} - \mathbf{r}'|} + E_{xc}[n] - \int v_{xc}\,(\mathbf{r})n(\mathbf{r})d\mathbf{r} \tag{45}$$

Equations 41, 43, and 44 are the central equations that encompass the Kohn-Sham formulation. These equations must be solved in an iterative, self-consistent process. A general procedure is outlined below.

1. Start with an initial, informed guess for the electron density.
2. Construct the V^{eff} equation.
3. Use the V^{eff} equation with the one-electron Schrodinger-like equation to determine the Kohn-Sham orbitals.
4. These orbitals are used to obtain a new density. This density is used as a new guess to repeat the process until a specified convergence is attained.
5. Once convergence is achieved, the total energy is calculated using the final electronic density.

Equation 45 could be solved for the exact ground-state energy and density if every term was known. In reality, the exchange-correlation functional term, E_{xc}, contains the quantum many-body electron-electron interactions and it is not known exactly. Therefore, approximations must be made to this functional.

Exchange-Correlation Functionals

The exact exchange-correlation functional is unknown and may never be known exactly. However, it is considerably well-studied and much is understood.[36] Another possible resolution is that the exact expression for the exchange-correlation functional will demand computational resources that are on the same order as the configuration interaction approach. In any case, certain approximations, each with their own advantages and

disadvantages, have been developed that describe the electronic system to varying degrees of accuracy.

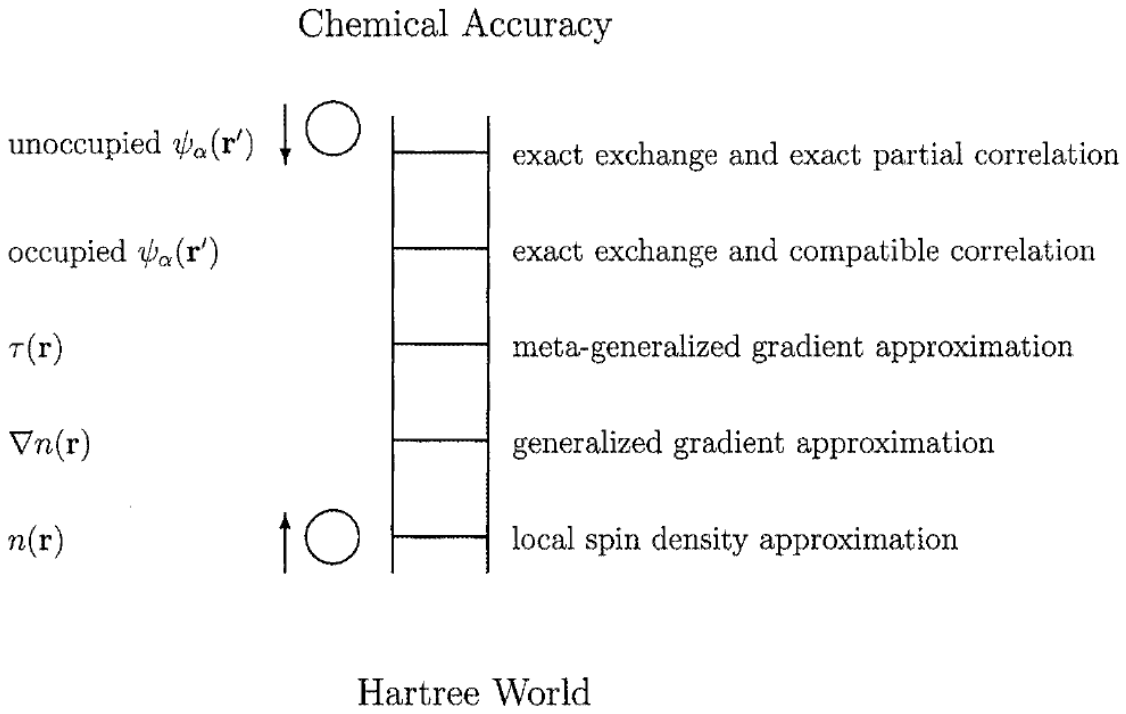

Figure 2: Jacob's Ladder depiction of exchange correlation functionals of increasing complexity.

A framework was developed by John Perdew and Karla Schmidt for organizing the myriad of different exchange-correlation functionals that exist.[37] This scheme imagines the rungs of a ladder as exchange-correlation functionals of increasing complexity. At the bottom is the Hartree-Fock theory while the top rung represents the ideal exact exchange-correlation energy. The common types of functionals along the ladder will be discussed. Local Density Approximation (LDA) is the first rung on the ladder followed by the Generalized Gradient Approximation (GGA), Meta-Generalized Gradient Approximation (Meta-GGA), and then hybrid functionals.

Local Density Approximation

For this approximation, an inhomogeneous system is divided into infinitesimal volumes where the electron density is assumed to be constant for each volume. Next, the exchange-correlation energy for each volume is assumed to be the same as the exchange-correlation energy obtained for the uniform electron gas for that density.[38,39] The total exchange-correlation energy can be written as (Equation 46).

$$E_{xc}^{LDA}[n] = \int n(\mathbf{r})\epsilon_{xc}^{unif}\big(n(\mathbf{r})\big)d\mathbf{r} \tag{46}$$

Here ϵ_{xc}^{unif} is the exchange-correlation energy per particle of an interacting uniform electron gas of density $n(\mathbf{r})$. In application, the exchange energy and correlation energy are calculated separately. In fact, it is often defined as (Equation 47).

$$E_{xc}^{LDA}[n] = E_{x}^{LDA}[n] + E_{c}^{LDA}[n] \tag{47}$$

The expression for the exchange energy is known exactly (Equation 48).

$$E_{x}^{LDA}[n] = -\frac{3}{4}\left(\frac{3}{\pi}\right)^{1/3}\int n^{4/3}(\mathbf{r})d\mathbf{r} \tag{48}$$

An analytic expression for the correlation energy is not known except in the limiting cases of weak and strong correlation.[32] However, intermediate density values have been computed by Monte Carlo methods.[39] The most successful exchange-correlation functionals have used the results from the Monte Carlo computations while also reproducing the limiting cases.[40–43] Initially, the LDA was not expected to perform well as an approximation for the exchange and correlation effects. However, at least for metals, a fortuitous cancellation of errors in the exchange and correlation terms lead to relatively good results. For other materials which do not have an inherent electronic structure that resembles a homogeneous electron gas, the LDA performs more poorly. For example, in

the LDA, the band gap for insulators tends to be underestimated by 20%-50%. Even with these issues, the relative simplicity of the LDA formalism, the explicit theoretical attachment of the LDA to an exactly treatable concept (the homogeneous electron gas), and the predictable consistency of trends in its errors have led the LDA (and its spin polarized form, the Local Spin-Density Approximation (LSDA)) to continue to be a widely used method of approximating the exchange and correlation effects in a wide range of materials.

Generalized Gradient Approximation

While the Local Density Approximation works well for systems of slowly varying densities, most real systems do not have slowly varying electron densities. In fact, the electron densities around atoms are quite inhomogeneous and as a result the LDA has systematic errors. In an attempt to overcome those errors, an extension to the LDA was proposed almost from the outset that incorporates the gradient of the electron density.[13] The Generalized Gradient Approximation (GGA) employs the electronic density as well as the gradient of the electronic density. However, because a suitable reference system does not exist for GGA in the same way that the homogeneous electron gas does for the LDA, a number of possible GGA forms have been developed.[44] A general form of these functionals resembles (Equation 49).

$$E_{xc}^{GGA}[n] = \int f^{GGA}\left(n(\mathbf{r}), \nabla n(\mathbf{r})\right) d\mathbf{r} \tag{49}$$

These functionals are called "semi-local" functionals in comparison to the LDA local approach. The form of f^{GGA} is used as a correction to the LDA exchange and correlation energies. The exchange energy looks like (Equation 50).

$$E_x^{GGA}[n] = \int n(\mathbf{r})\epsilon_x^{unif}\left(n(\mathbf{r})\right)F_x^{GGA}(s)d\mathbf{r} \tag{50}$$

Here $F_x^{GGA}(s)$ is called the exchange enhancement factor. This indicates how much exchange energy is added beyond the LDA value for a given $n(\mathbf{r})$. The argument of the exchange enhancement factor, *s*, is defined to be (Equation 51).

$$s = \frac{|\nabla n(\mathbf{r})|}{2(3\pi^2)^{\frac{1}{3}}n^{\frac{4}{3}}(\mathbf{r})} \tag{51}$$

Of particular interest in the development of an accurate GGA is consideration of the conditions and limits on its form.[45] One exact condition for GGA is that $E_{xc}[n]$ reduce to the gradient expansion approximation when the density is slowly-varying. Others require that $E_{xc}[n]$ reduce to the LDA when the density is uniform and the exchange-correlation hole is normalized. Additionally, coordinate scaling conditions that address the high and low electron density limits can be imposed which satisfy a different set of conditions.

Meta-Generalized Gradient Approximations

The next functionals on the ladder add the kinetic energy density, $\tau_\sigma(r)$, to the local density of the LDA and the gradient density of the GGA.[46] The kinetic energy density is the second derivative of the electronic density (Equation 52).

$$\tau_\sigma(n) = \sum_i^{occup} \frac{1}{2}|\nabla\psi_{i\sigma}(\mathbf{r})|^2 \tag{52}$$

Here the kinetic energy density is incorporated into the exchange-correlation functional to complete the third rung of Jacob's ladder (Equation 53).

$$E_{xc}[n_\uparrow, n_\downarrow] = \int d^3r n\epsilon_{xc}(n_\uparrow, n_\downarrow, \nabla n_\uparrow, \nabla n_\downarrow, \tau_\uparrow, \tau_\downarrow) \tag{53}$$

Where $n(r) = n_{\uparrow}(r) + n_{\downarrow}(r)$ is the total density and $n_{\uparrow}(r)$ and $n_{\downarrow}(r)$ are the spin-up and spin-down densities, respectively. The extra degree of freedom provided by the kinetic energy density term has been used to satisfy additional constraints on the exchange-correlation functional such as a self-interaction corrected correlation functional, recovery of the fourth-order gradient expansion in the limit of slowly varying densities, and a finite exchange potential at the nucleus.

Hybrid Functionals

Hybrid functionals represent functionals that incorporate exact exchange from the Hartree-Fock calculations. A key formula used in hybrid functionals is (Equation 54).

$$E_{xc} = \int_0^1 U_{xc}^{\lambda}\, d\lambda \tag{54}$$

Here λ is a parameter controlling the inter-electronic coupling strength related to the Coulomb repulsion. The potential energy of exchange and correlation for a given λ is U_{xc}^{λ}. This formula links together a non-interacting system with a fully interacting system at an electronic density $n(\mathbf{r})$.

The Hubbard Model

The Hubbard Model is an approximation for interacting electrons introduced by John Hubbard in a series of papers between 1963 and 1964.[47–49] In these papers, Hubbard proposed that the most dominant electron-electron interactions are between electrons that are bound to the same atom. This idea of strongly interacting or strongly correlated electrons has been used to describe ferromagnetism[50–52], antiferromagnetism[53,54], high-

temperature superconductivity[55,56], and the Mott metal-insulator transition.[57,58] The mathematical framework was initially presented as applying only to *s* orbitals, but was later expanded and generalized to account for interaction between electrons in *d* and *f* orbitals.

The Hubbard Hamiltonian takes the form (Equation 55)

$$H = -t \sum_{\langle i,j \rangle,\sigma} \left(c_{i,\sigma}^{\dagger} c_{j,\sigma} + c_{j,\sigma}^{\dagger} c_{i,\sigma} \right) + U \sum_{i=1}^{N} n_{i\uparrow} n_{i\downarrow} \tag{55}$$

where $\langle i, j \rangle$ indicates an interaction with the nearest-neighbor on a lattice. The raising and lowering operators are $c^{\dagger}$ and c, respectively. $n_{i\sigma}$ represents the number of electrons with a particular spin at an atomic site i. The first term embodies the kinetic energy of the electrons as they hop between their nearest neighbors; thus, it is often called the hopping integral. The second term describes the on-site Coulomb repulsion between electrons in the same atomic orbital. It is the Hubbard U parameter that is defined as the Coulomb energy cost to place two electrons at the same site (Equation 56).

$$U = E(d^{n+1}) + E(d^{n-1}) - 2E(d^{n}) \tag{56}$$

Two limits are discussed in Hubbard's papers: $U \gg t$ and $U \ll t$. In the $U \gg t$ limit the Hubbard U Coulomb repulsion overcomes the kinetic hopping energy and the material cannot move electrons from atomic site to atomic site; thus, resulting in an insulator. For the $U \ll t$ limit the kinetic hopping energy is dominant compared with the on-site Coulomb repulsion allowing for electrons to move to a nearest-neighbor. How the ratio of U/t varies is of interest because it can elucidate how the metal-insulator transition (and the Mott metal-insulator transition) occurs in transition metal complexes, specifically those with important 3d orbital character.

The work in this thesis extracts the concept of Hubbard on-site Coulomb repulsion and incorporates it into the energy calculations. Specific details are expanded upon in Chapter 3, but examples of recent work utilizing Hubbard U within the LDA framework are mentioned here. In the work of Anisimov et al.[59] an exchange-correlation potential was proposed for Mott insulators. The energy functional used the LDA plus a mean-field approximation for the Hubbard U term. It was found that all late-3d transition metal monoxides are large gap magnetic insulators of the charge-transfer type. Their version fails for early-3d transition metal monoxides and for late-3d transition metals. Liechtenstein et al.[60] applied the LDA plus Hubbard U to account for spin and orbital polarization as caused by on-site Coulomb interactions instead of exchange interactions of the homogeneous electron gas. They showed that the electronic orbital ordering was a necessary condition to obtain the correct crystal structure for the material of interest, the Mott-Hubbard insulator $KCuF_3$. Lastly, the linear combination of pseudo-atomic orbital (LCPAO) method has been used in conjunction with the LDA.[61] As opposed to an on-site representation of the occupation number matrix, a dual representation is presented leading the LDA+U formalism to be consistent with a non-orthogonal LCPAO basis. The band gap, magnetic properties, and electronic structure of numerous transition metal oxide systems were investigated with different choices of basis sets and effective U values. The LDA+U LCPAO method was found to be in good agreement with previous theoretical and experimental studies.

CHAPTER 3

THE ORTHOGONALIZED LINEAR COMBINATION OF ATOMIC ORBITALS METHOD

The Orthogonalized Linear Combination of Atomic Orbitals (OLCAO) method is a set programs based on density functional theory. The developed features of the method have found use in studying large periodic systems such as amorphous solids, complex crystals, and biological molecules. The history, theory, and applications of the method can be found in *Electronic Structure Methods for Complex Materials: The Orthogonalized Linear Combination of Atomic Orbitals* by Ching and Rulis.[62] The OLCAO method uses atomic orbitals as the basis functions for a Bloch sum (Equation 57).

$$u_i(\mathbf{r}) = \left[\sum_{j=1}^{N} A_j\, r^l e^{(-\alpha_j r^2)}\right] \cdot Y_l^m(\theta, \phi) \tag{57}$$

In the atomic orbital function $u_i(\mathbf{r})$ the term in the square brackets is the Gaussian-type orbital (GTO) radial part and the Y_l^m function is the angular part. The radial term is a linear combination of GTOs while Y_l^m represent the normal real spherical harmonics. Here, i represents a set of quantum numbers, A_j is an expansion coefficient, and α_j is a decay exponent. The decay exponent is usually chosen as a set of values that varies from element to element and is determined from past test calculations. These atomic basis functions are used to construct a Bloch sum (Equation 58).

$$b_{i\gamma}(\mathbf{k}, \mathbf{r}) = \left(\frac{1}{\sqrt{N}}\right) \sum_{\upsilon} e^{i(\mathbf{k}\cdot\mathbf{R}_\upsilon)}\, u_i(\mathbf{r} - \mathbf{R}_\upsilon - \mathbf{t}_\gamma) \tag{58}$$

In the Bloch sum the atomic basis functions are centered at different atomic site and combined linearly. The set of quantum numbers is again denoted by i, γ labels the atoms in a cell, and **k** is the wave vector. Besides the radius r in the atomic basis function,

$\mathbf{R}_\upsilon$ is the lattice vector and $\mathbf{t}_\gamma$ is the position of the atomic site designated by γ. The final step to achieve the solid state wave function is to assemble the Bloch sums in a linear combination (Equation 59)

$$\Psi_{n\mathbf{k}}(\mathbf{r}) = \sum_{i,\gamma} C_{i\gamma}^{n}(\mathbf{k}) b_{i\gamma}(\mathbf{k}, \mathbf{r}) \tag{59}$$

where n is the band index or energy levels and $C_{i\gamma}^{n}$ is the expansion coefficient.

The basis functions are divided into two groups, core and valence. The core atomic orbital basis functions are generally those with a binding energy of -30 eV or deeper and the valence orbitals are all the remaining basis functions. The number of basis functions to use depends on the accuracy needed or the property of interest to be calculated. For convenience, the OLCAO method uses three main groupings of basis set functions. First, the minimal basis set includes the core orbitals and then only the occupied valence shell orbitals designated by n and l quantum numbers. (Note that for an element such as boron which has one electron in a 2p-orbital, the minimal basis would include the 1s, 2s, and $2p_x$, $2p_y$, and $2p_z$ orbitals. As a consequence, some minimal basis orbitals will be unoccupied.) Second, the full basis set adds empty orbitals of the next higher n quantum number for each of the occupied type of angular momentum quantum numbers. As an example, the full basis for boron would include the 3s and 3p orbitals, but not 3d. Third, the extended basis set adds yet again the next higher n quantum number orbitals. Therefore, the extended basis for boron would include 4s and 4p orbitals, but again not 3d or 4d. This description should be interpreted as a rule of thumb that defines the default set of basis sets for each element and not a hard and fast requirement. There are some cases, such as for silicon, where the extra variational freedom introduced by the inclusion of unoccupied 3d orbitals in the full

basis set is necessary for achieving the desired accuracy. These variations have been built up through experience and testing of the method over many years.

Modifications to OLCAO code

As discussed at the end of Chapter 2 the modifications to the OLCAO code are focused on borrowing concepts from the Hubbard Hamiltonian and an orbital-dependent on-site potential presented by Anisimov et al. The idea of an on-site Coulomb repulsion parameter, the Hubbard U, is incorporated into an LSDA potential (Equation 60)

$$V_{im\sigma} = V^{LDA} + U\sum_{m'}(n_{im'-\sigma} - n^0) + (U-J)\sum_{m\prime\neq m}(n_{im\prime\sigma} - n^0) \qquad (60)$$

where m and m' denote orbitals, i and σ specify the atom and the spin, and $(n_{im\prime\sigma} - n^0)$ represents the deviation of the electron number in the m'th orbital of the ith atom from the average electron number n^0. Additionally, V^{LDA} is the usual LSDA potential, U is the Hubbard parameter and J is a Hund's rule exchange parameter. For Fe-TCNE it is expected that Fe^{II} and $[TCNE]^{\bullet-}$ will be the largest contributors to magnetic ordering. For calculations performed in this work, the average electron number $n^0 = 6/10$ since there are six Fe 3d electrons to be placed across the ten possible spin states. Typically, Hubbard U is on the order of 10 eV while the Hund's rule J is on the order of 1 eV.[59] Modifications were made primarily in the potential.f90 and secularEqn.F90 files of the OLCAO code to include the Anisimov potential, to identify how the +UJ terms were applied, and to control how the input and output of those files interacted with the larger OLCAO program structure.

CHAPTER 4
RESULTS AND DISCUSSION

Fe-TCNE and Hubbard U

Atomic Structure

The organic-based magnet $[Fe^{II}(TCNE)(NCMe)_2][Fe^{III}Cl_4]$, where Me = methyl, has a layered magnetic structure with MeCN ligands separating the layers. The Fe^{II} ion bonds to four TCNE anions while two MeCN ligands bond perpendicularly to the Fe^{II} ion. The $Fe^{III}Cl_4$ anion is located between the layers. The magnetic behavior orders as a ferrimagnet below a $T_c = 90$ K and spin polarization has been experimentally reported. Fe-TCNE has an orthorhombic cell with several different types of atoms depending on an atom's particular species or position within the cell. There two types of Fe (Fe^{II} and Fe^{III}, as mentioned above), seven types of C, four types of N, three types of Cl, and six types of H; this totals to 112 atoms. Crystallographic structure information was obtained from a cif file available online from the Crystallography Open Database.[15] The unit cell has a, b, and c vector values of 14.3327 Å, 16.482 Å, and 7.28 Å. The α, β, and γ angles are all 90° and the Hermann-Mauguin space group is *Pnam*.

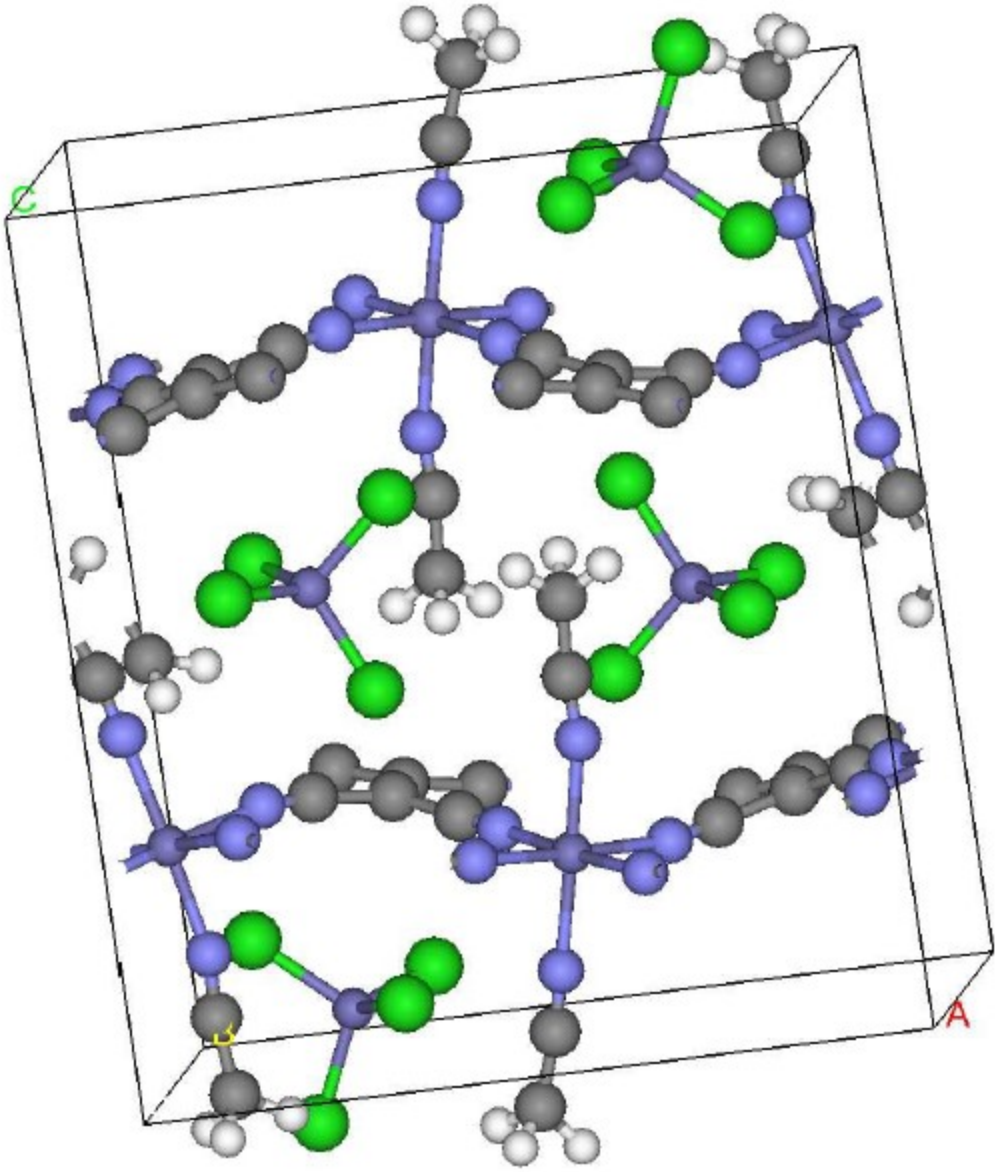

Figure 3: Crystal structure of Fe-TCNE.

Calculations were performed for Fe-TNCE to demonstrate self-consistent convergence before application of the Hubbard U parameter. A full basis set containing atomic orbitals of Fe ([Ar] core plus 3d,4s,4p,5s,5p,4d), N (1s,2s,2p,3s,3p) C (1s,2s,2p,3s,3p) and H (1s,2s,2p) was used for the calculations. In order to aid the analysis

of the partial density of states (PDOS), the b and c axes were exchanged within the olcao.skl skeleton file. This was done so as to allow the Fe^{II} d_z^2 orbital to better align with the unit cell axes. To decrease the computational time required the number of ***k*** point vectors prior to performing symmetry operations were used. Moreover, this allowed for the removal of extra H atoms on the methyl groups before they even appeared, an error caused during the symmetry operations. Note that once the makeinput command is given the space group is changed to *P1*. This was captured in the olcao.skl file before any calculations were made. A convergence limit of 0.0001 or less was achieved with a ***k*** point mesh of 5 x 10 x 5 for both the self-consistent field and post-self-consistent parts. A comparison of convergence data is presented in the +UJ paragraphs below. Spin polarization was turned on within the program and a thermal smearing value of 0.8 eV was used. A feedback level of 4 and a relaxation factor of 0.15 and 0.1 was selected. The Fe^{II} ions (Fe type 1) were identified to have a spin splitting factor of 0.3 Bohr magnetons with spin splitting set to 0.0 Bohr magnetons for all other atoms. Finally, the exchange correlation functional used was per Ceperley-Alder and the U and J values were 4.0 eV and 0.0 eV, respectively.

Electronic Properties

Partial Density of States

The partial density of states obtained for Fe-TCNE prior to +UJ application is presented and described below for various parts of the material.

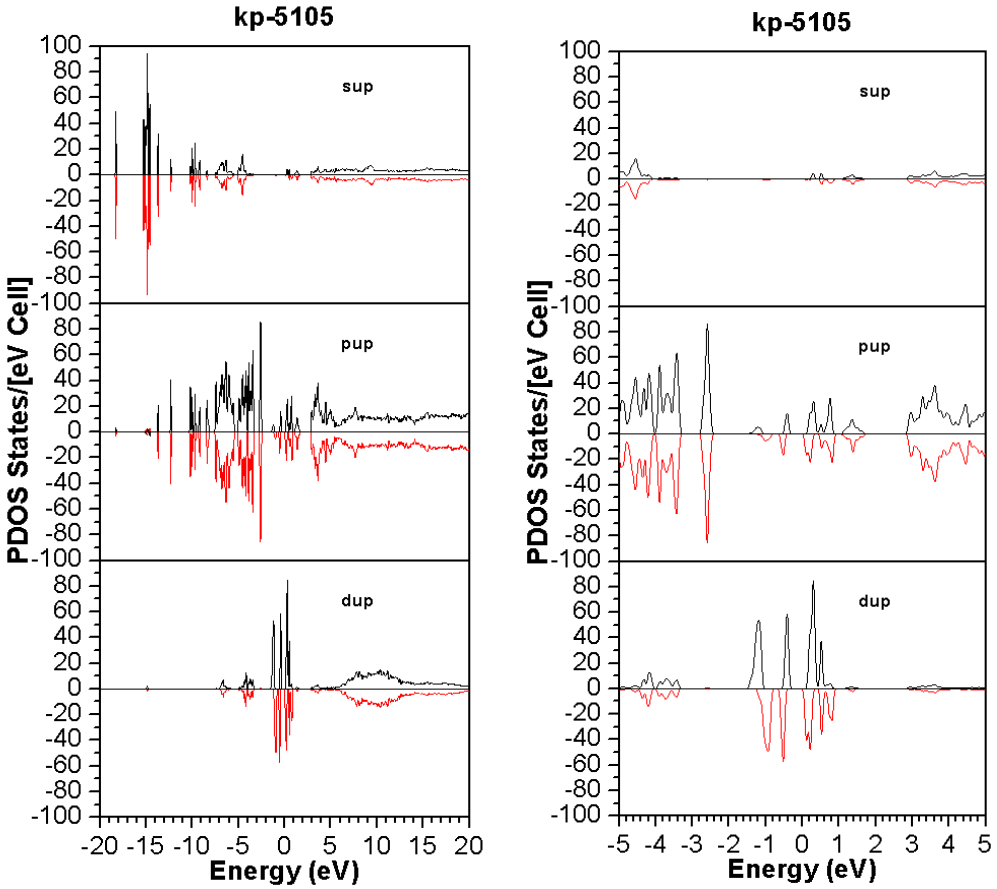

Figure 4: (Left) PDOS of *s*, *p*, and *d* orbitals for all atoms. (Right) PDOS of *s*, *p*, and *d* orbitals for all atoms in an x range of -5 eV to +5 eV.

Figure 4 showcases an overall view of the spin up and spin down density of states of *s*, *p*, and *d* orbitals for all atoms. The largest contributors to the density of states are the electrons residing in the *p* and *d* orbitals. Considering the narrow view of the PDOS (Figure 4, Right) gives a better indication of how the *p* and *d* orbitals behave close to the Fermi energy. One can observe that there is spin splitting near the Fermi energy and that *d* orbital behavior is the most prominent. This is a good indication that correctly describing the *d* orbital behavior close to the Fermi energy will provide a better result for the band gap.

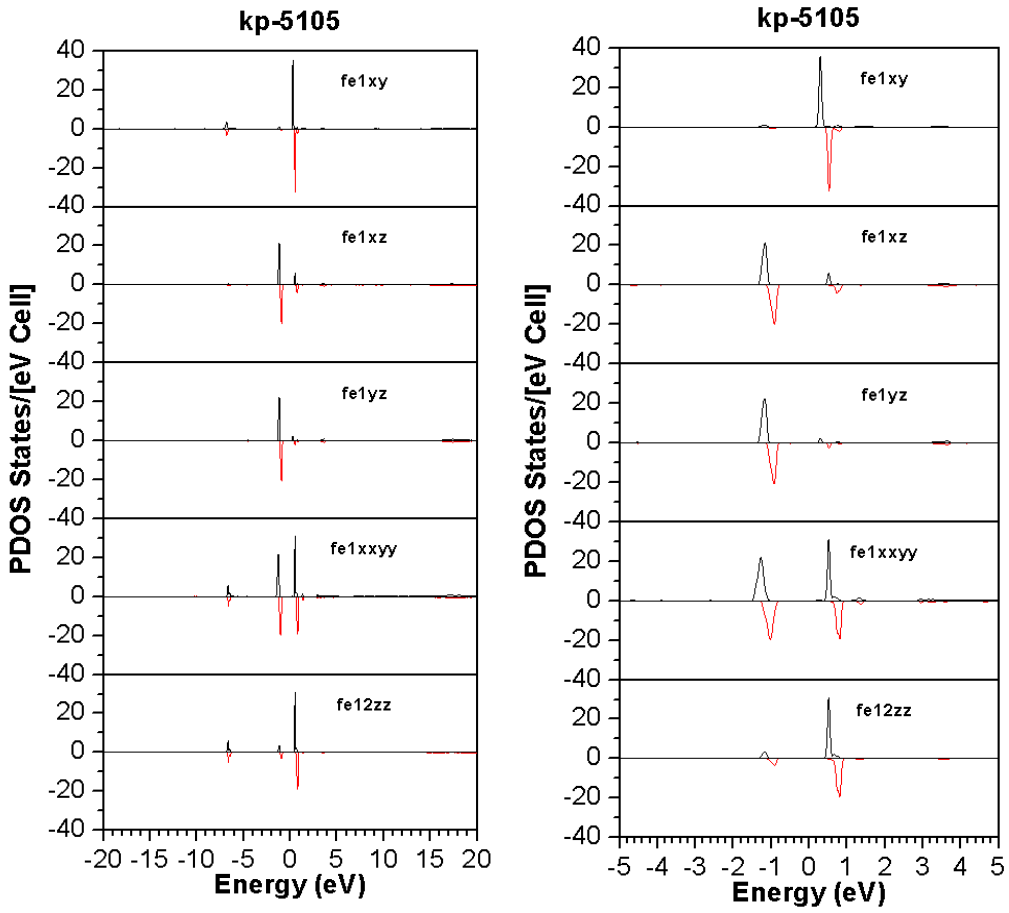

Figure 5: (Left) PDOS of Fe^{II} *d* orbitals. (Right) PDOS of Fe^{II} *d* orbitals in an x range of -5 eV to +5 eV.

Figure 5 shows the PDOS of the Fe^{II} *d* orbitals. Recall that the Fe^{II} atoms are part of the TCNE layer and thought to add the most to the magnetic ordering. In fact, looking at the following figures for the other atom types it is clear that they do not greatly influence behavior at the Fermi level. Focusing on the narrow view (Figure 5, Right), the most important *d* orbitals are d_{xy}, $d_{x^2-y^2}$, and d_{z^2}. Contributions from orbitals d_{xz} and d_{yz} are minimal. Spin splitting is evident for all orbitals.

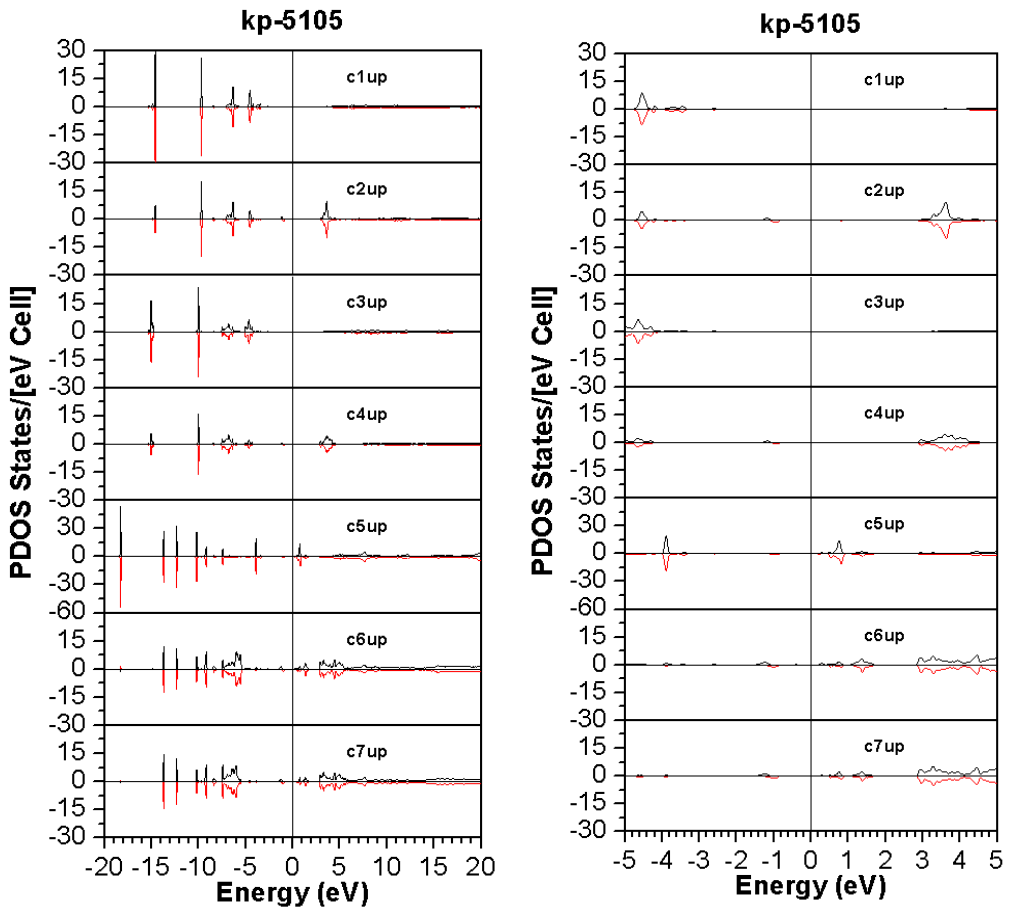

Figure 6: (Left) PDOS for all C types. (Right) PDOS for all C types in an x range of -5 eV to +5 eV.

Figure 6 shows the PDOS for all C atom types. The C atom types have a low number of states and almost no spin splitting is observed.

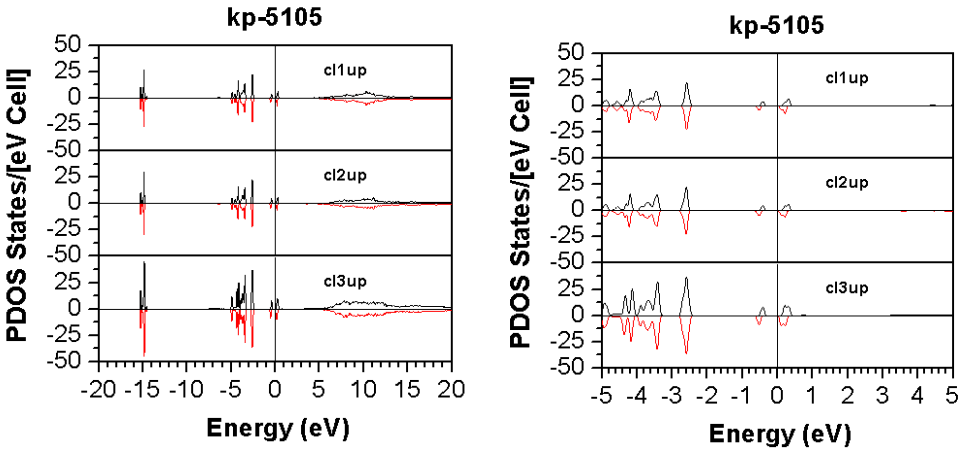

Figure 7: (Left) PDOS for all Cl types. (Right) PDOS for all Cl types in an x range of -5 eV to +5 eV.

Figure 7 shows the PDOS for all Cl atom types. A small amount of spin splitting is observed, but there is little indication that it contributes to the overall magnetism.

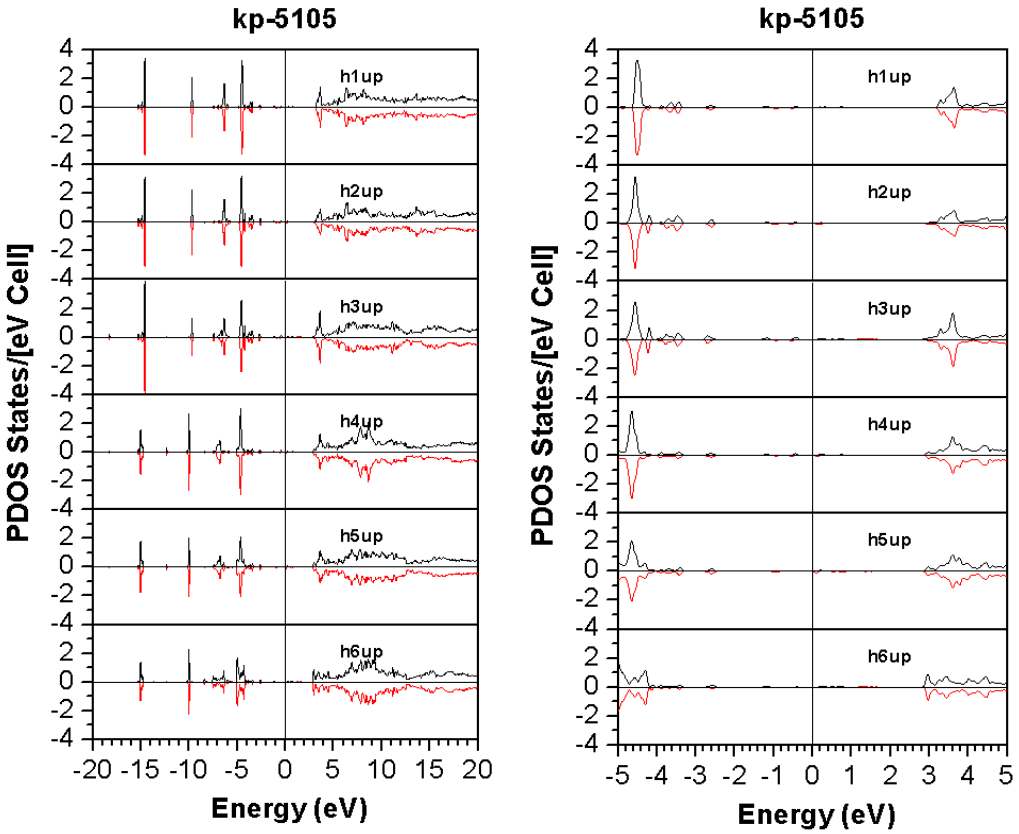

Figure 8: (Left) PDOS for all H types. (Right) PDOS for all H types in an x range of -5 eV to +5 eV.

Figure 8 shows the PDOS for all H types. The density of states for all H atom types are far away from the Fermi energy and do not indicate any contribution to magnetic ordering.

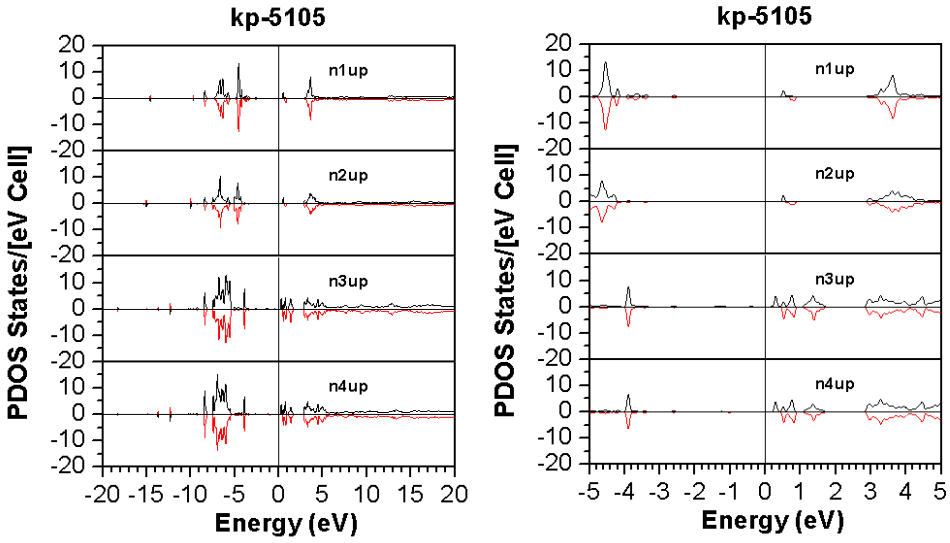

Figure 9: (Left) PDOS for all N types. (Right) PDOS for all N types in an x range of -5 eV to +5 eV.

Figure 9 shows the PDOS for all N types. Spin splitting is observed for the N types within 2 eV of the Fermi energy, but the density of states is low.

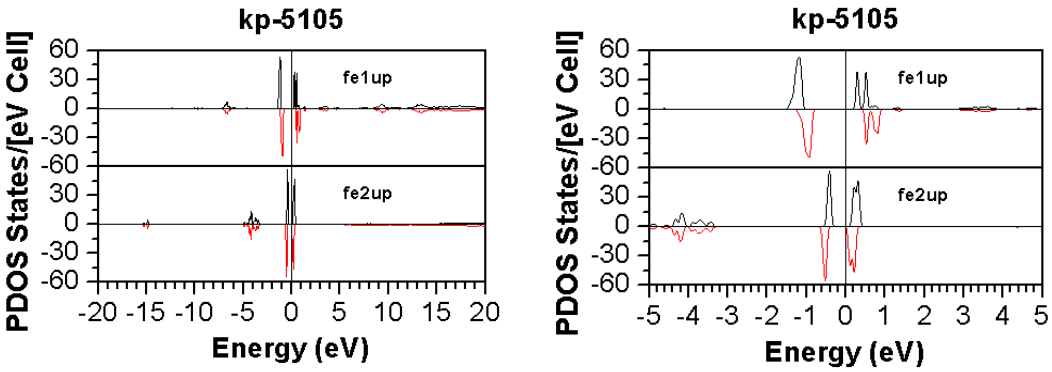

Figure 10: (Left) PDOS for all Fe types. (Right) PDOS for all Fe types in an x range of -5 eV to +5 eV.

Figure 10 shows a comparison of the PDOS for Fe types 1 and 2; i.e, the Fe^{II} and Fe^{III} species. The most interesting behavior occurs close to the Fermi energy. Spin splitting is apparent for both Fe types, but the Fe^{II} species exhibits more than the Fe^{III} species. It is expected that once the +UJ is applied that the distance between the density of states for Fe^{II} will increase.

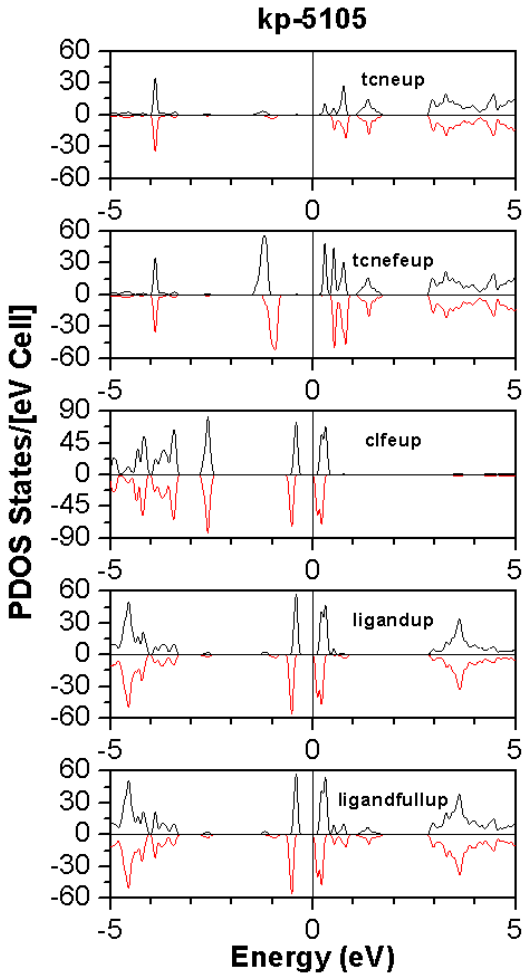

Figure 11: PDOS for various sections of the Fe-TCNE structure. (From top to bottom) TCNE, TCNE and the Fe^{II} ion, Cl atoms and Fe^{III} ion, NCMe ligands, and NCMe ligands with Fe^{II} ions.

Figure 11 shows the PDOS for various sections of Fe-TCNE; specifically, TCNE itself, TCNE and Fe^{II}, Cl atoms and Fe^{III}, the NCMe ligands, and the NCMe ligands with Fe^{II} atoms. The TCNE and TCNE with Fe^{II} show spin splitting near the Fermi edge. As would be expected with the TCNE/Fe^{II} fragment, the Fe^{II} atoms increase the spin up and spin down density of states values. The Cl/Fe^{III} portion show spin splitting near the Fermi level. The NCMe and NCMe/Fe^{II} ligands are very similar; the only difference being some extra states between approximately 0.5 eV and 2.0 eV because of Fe^{II}.

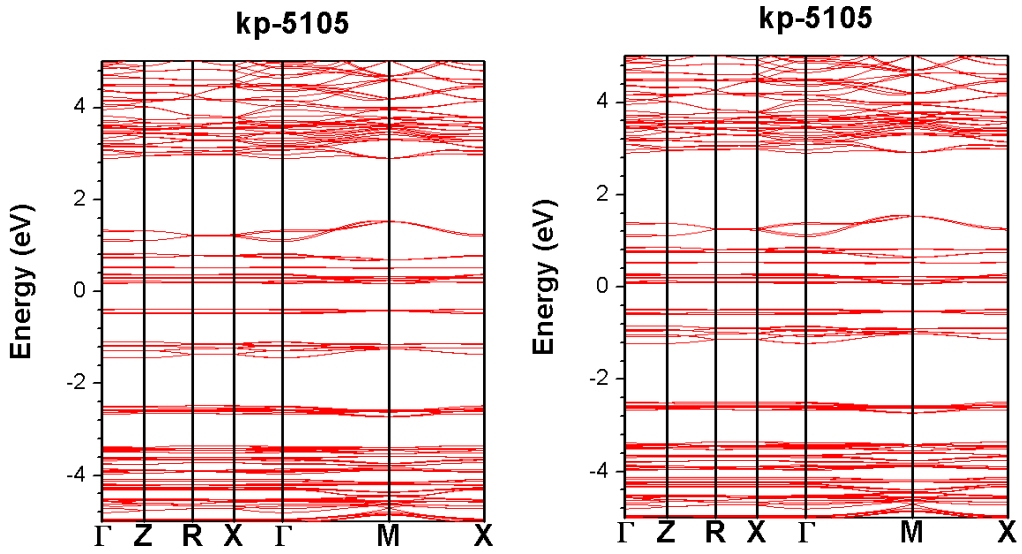

Figure 12: (Left) Symmetric band structure for spin up. (Right) Symmetric band structure for spin down.

The overall symmetric band structure for spin up and spin down is shown in Figure 12. The plots are extremely similar; however, one can observe that the bands near the Fermi energy are slightly different, specifically between 0.8 eV and -0.8 eV. A band gap of approximately 1.2 eV is observed which is an increase from the 0.04 eV previously reported.[17]

Partial Density of States with +UJ Application

The partial density of states obtained for Fe-TCNE with +UJ applied is presented and described below for various parts of the material. The Hubbard U and Hund's J values were treated as adjustable parameters instead of being calculated from a first principles approach. A Hubbard U value of 4.0 eV and a Hund's J exchange value of 0.0 eV were selected. In addition, convergence data is included for calculations before and after +UJ. Data shows that the time to convergence improved when using the +UJ values.

Table 1: Convergence data for Fe-TCNE without +UJ treatment.

Iter.	Occ. Energy	El. Error	Convergence	Total Energy	Mag. Mom.
1	-0.15676879	1.21374156	0.19662469	-887.1904188	41.81787982
2	-0.16765499	1.27301315	0.3040938	-886.6629936	2.42830425
3	-0.16551732	1.28999566	0.06900151	-887.5071279	2.10926838
4	-0.16108167	1.26830503	0.05615799	-887.5149899	2.08601905
5	-0.16171816	1.27870685	0.01838237	-887.5716371	2.06081079
6	-0.16129848	1.28615934	0.02402915	-887.5848327	2.0031105
7	-0.15995796	1.30350543	0.07771205	-887.5221402	1.96789015
8	-0.16071731	1.29321721	0.01639605	-887.5988815	1.96888924
9	-0.16019068	1.29631368	0.00891	-887.6041191	1.96078598
10	-0.15940588	1.30197904	0.00842881	-887.6102868	1.8872401
11	-0.15749843	1.31353258	0.01693501	-887.6167348	1.71367775
12	-0.15861984	1.30600827	0.00480382	-887.6136225	1.77975557
13	-0.15830331	1.30810957	0.00213695	-887.6152564	1.75200608
14	-0.15795193	1.30959059	0.00340042	-887.6159445	1.70089823
15	-0.15802789	1.30999752	0.00581299	-887.6155186	1.76821797
16	-0.15791126	1.31015473	0.00106719	-887.616245	1.74034663
17	-0.15782753	1.31051921	0.00102608	-887.6163855	1.76074165
18	-0.15744353	1.31214291	0.00432904	-887.6170335	1.9029543
19	-0.15768551	1.31128764	0.00151319	-887.6167673	1.84506742
20	-0.15757621	1.31173239	0.00061663	-887.6170534	1.88676441
21	-0.15748091	1.312248	0.00079018	-887.6173742	1.94793818
22	-0.15745773	1.31208202	0.00261656	-887.6172442	1.94907805
23	-0.15745604	1.3122874	0.00026191	-887.6174348	1.95657478
24	-0.15743974	1.31236471	0.00027729	-887.6174969	1.96348647
25	-0.15733388	1.31293256	0.00096326	-887.6178802	1.99929449
26	-0.15740234	1.31250124	0.0006954	-887.6176074	1.95755517
27	-0.15736634	1.31269366	0.00024328	-887.617741	1.97544051
28	-0.15734172	1.31280457	0.00025984	-887.6178208	1.98290553
29	-0.15731599	1.3129899	0.00077211	-887.6179163	2.00522406
30	-0.15733114	1.31286064	0.00008043	-887.617855	1.9934547

Table 2: Convergence data for Fe-TCNE with +UJ treatment.

Iter.	Occ. Energy	El. Error	Convergence	Total Energy	Mag. Mom.
1	-0.15751782	1.31291686	0.0375936	-887.7578177	43.59090837
2	-0.15679734	1.31537962	0.05801262	-887.5818415	9.0436327
3	-0.15712567	1.31285589	0.0043624	-887.6219067	8.80633514
4	-0.15714578	1.31357422	0.00787349	-887.6214952	8.78706804
5	-0.15714568	1.31352166	0.00778496	-887.6215825	8.80075705
6	-0.15686279	1.31305687	0.02397159	-887.616744	9.23880954
7	-0.15723263	1.31318318	0.00208006	-887.6219349	8.6253827
8	-0.15718845	1.31345403	0.00330438	-887.6218195	8.64773801
9	-0.15721594	1.31341828	0.00126467	-887.6219639	8.61980612
10	-0.15721011	1.31337173	0.001064	-887.6218742	8.60956347
11	-0.15725763	1.31344225	0.00143569	-887.6219649	8.59611553
12	-0.15721865	1.31337405	0.00045237	-887.6218631	8.60892344
13	-0.15722857	1.31337698	0.00021924	-887.6219066	8.61523087
14	-0.15722596	1.31338544	0.00018068	-887.6219035	8.62188423
15	-0.15722599	1.3133667	0.00013191	-887.6219076	8.62768737
16	-0.1572273	1.31338839	0.00012995	-887.6219198	8.63712428
17	-0.15722484	1.31334215	0.0001471	-887.6219175	8.64562157
18	-0.1572277	1.31337877	0.00010835	-887.621934	8.65307926
19	-0.15722483	1.31335433	0.0001095	-887.6219321	8.66602911
20	-0.15722976	1.31337769	0.00014695	-887.6219687	8.68090692
21	-0.15722681	1.31337149	0.00011879	-887.6219587	8.68236918
22	-0.15722622	1.3133554	0.00009493	-887.6219619	8.69057788

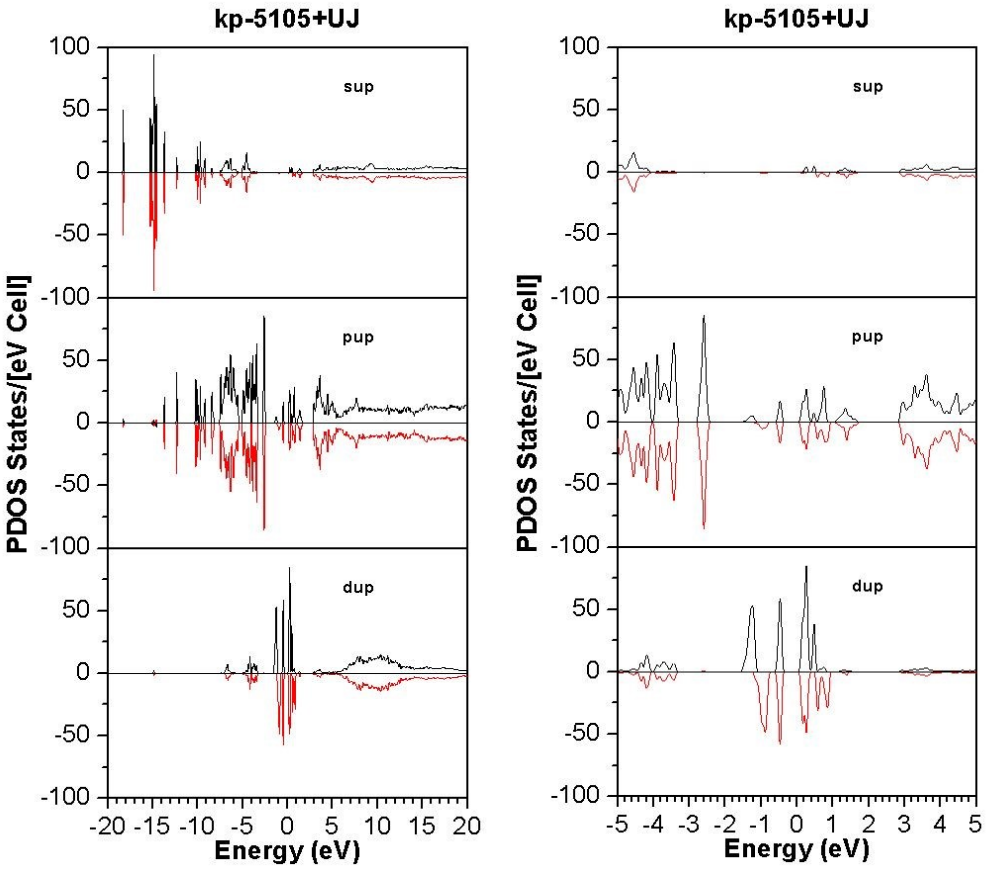

Figure 13: (Left) PDOS of *s*, *p*, and *d* orbitals for all atoms. (Right) PDOS of *s*, *p*, and *d* orbitals for all atoms in an x range of -5 eV to +5 eV.

Figure 13 showcases an overall view of the spin up and spin down density of states of *s*, *p*, and *d* orbitals for all atoms. The largest contributors to the density of states are the electrons residing in the *p* and *d* orbitals. Considering the narrow view of the PDOS (Figure 13, Right) gives a better indication of how the *p* and *d* orbitals behave close to the Fermi energy. One can observe that there is spin splitting near the Fermi energy and that *d* orbital behavior is the most prominent.

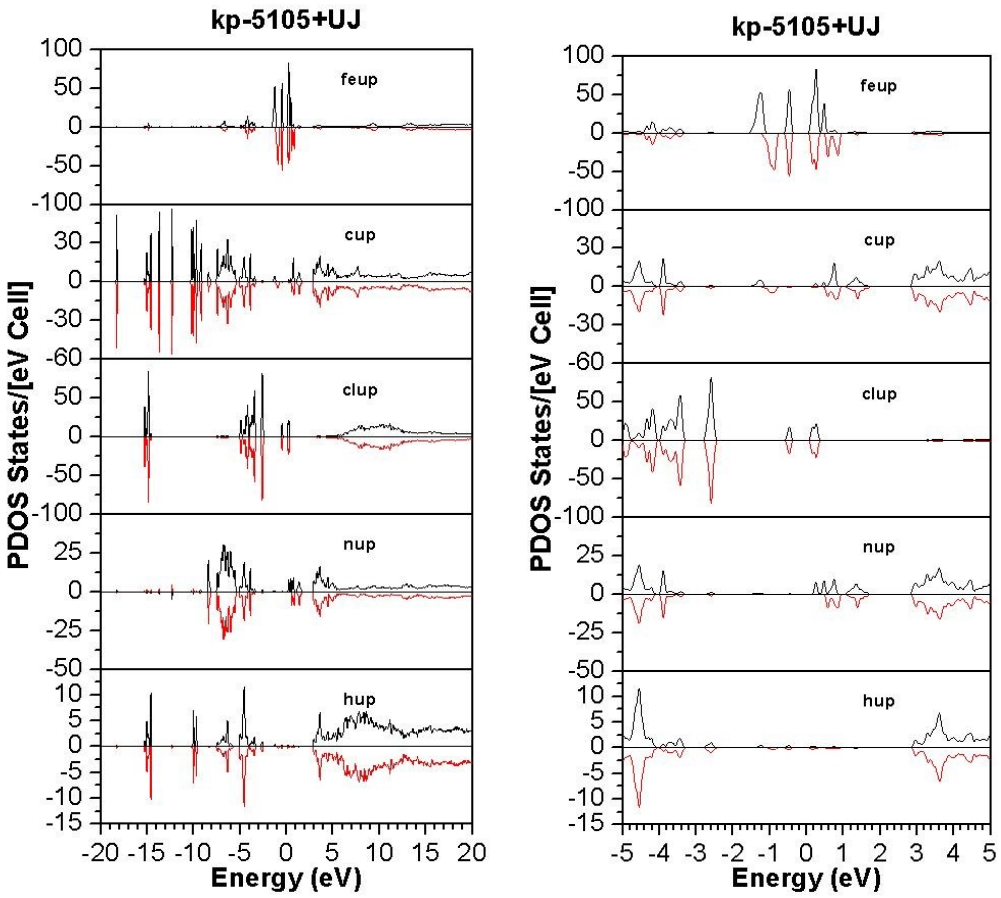

Figure 14: (Left) PDOS of all elements with +UJ. (Right) PDOS of all elements with +UJ in an x range of -5 eV to +5 eV.

Figure 14 shows the PDOS of all elements with +UJ applied. Spin splitting is most obvious for the Fe, Cu, and N elements close to the Fermi level. Also, the Fe element displays the highest density of states.

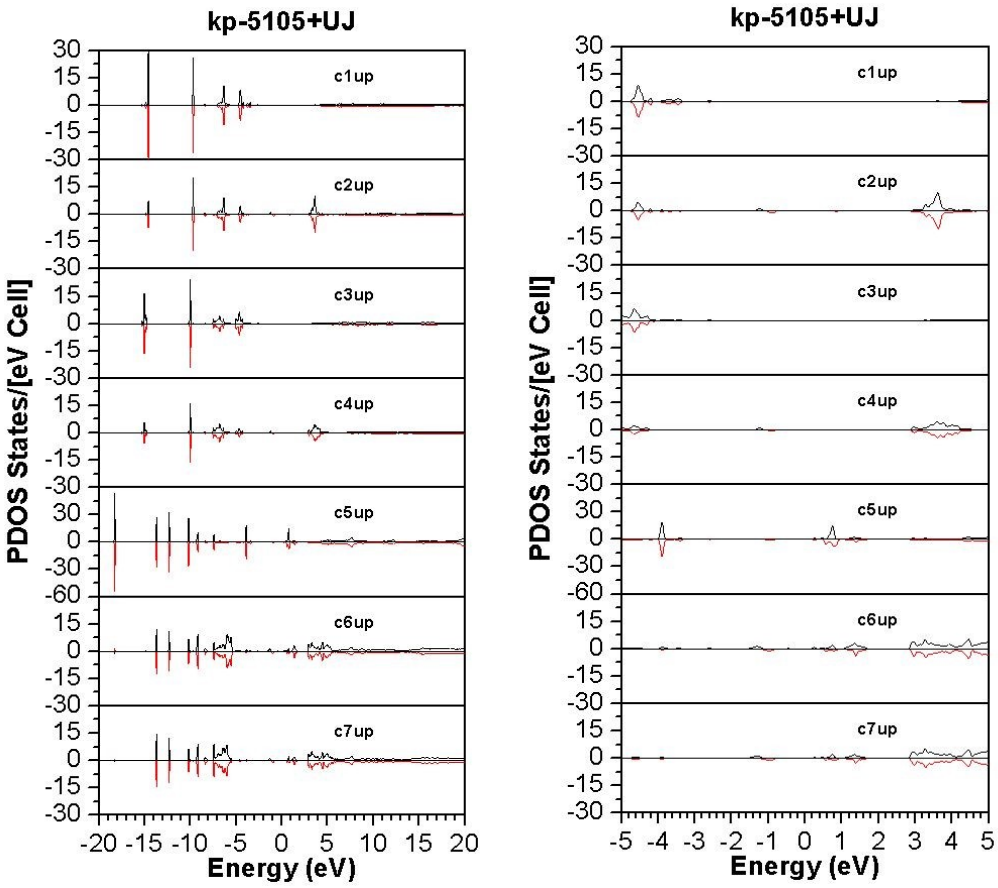

Figure 15: (Left) PDOS for all C types with +UJ. (Right) PDOS for all C types with +UJ in an x range of -5 eV to +5 eV.

Figure 15 shows the PDOS for all C atom types with +UJ applied. The C atom types have a low number of states and little spin splitting is observed.

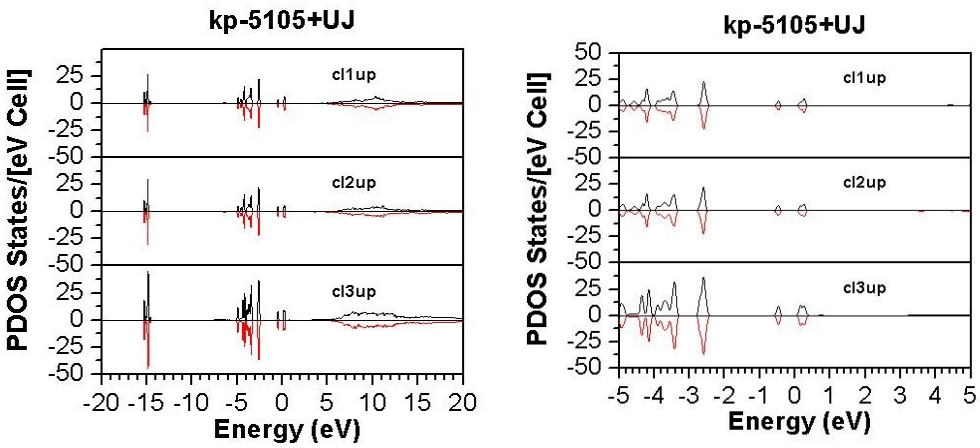

Figure 16: (Left) PDOS for all Cl types with +UJ. (Right) PDOS for all Cl types with +UJ in an x range of -5 eV to +5 eV.

Figure 16 shows the PDOS for all Cl atom types with +UJ. There is no obvious sign of spin splitting for any of the Cl atoms.

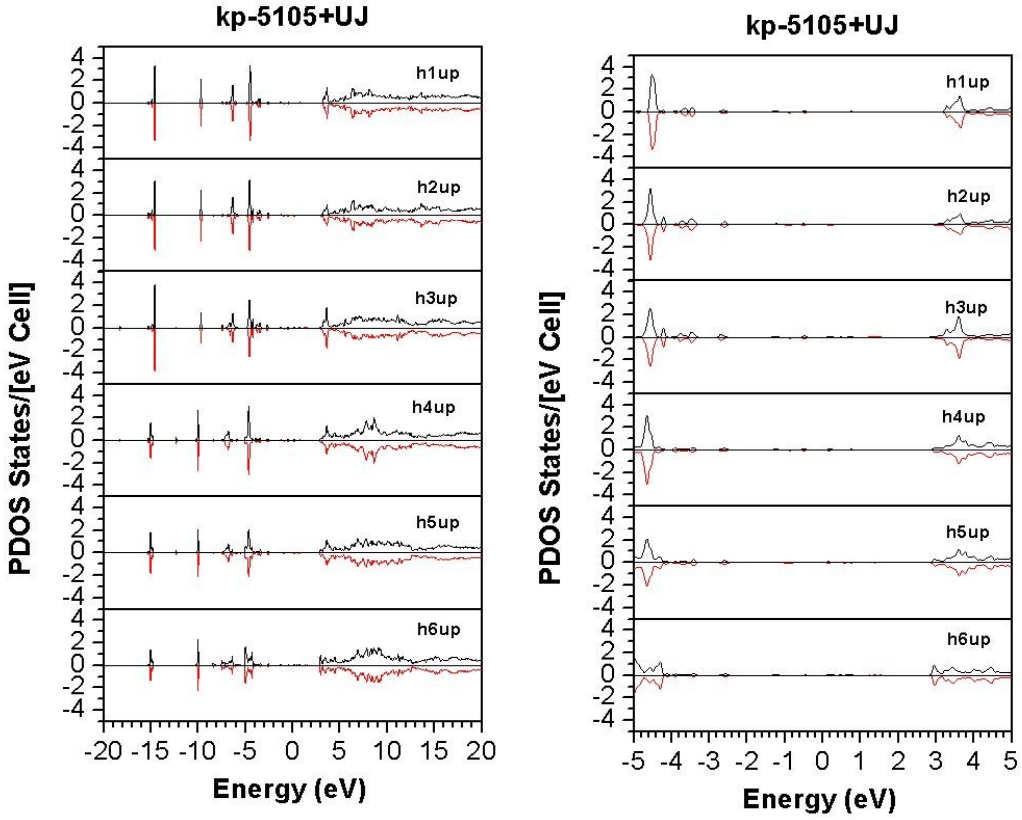

Figure 17: (Left) PDOS for all H types with +UJ. (Right) PDOS for all H types with +UJ in an x range of -5 eV to +5 eV.

Figure 17 shows the PDOS for all H types with +UJ. The density of states for all H atom types are far away from the Fermi energy and do not indicate any contribution to magnetic ordering.

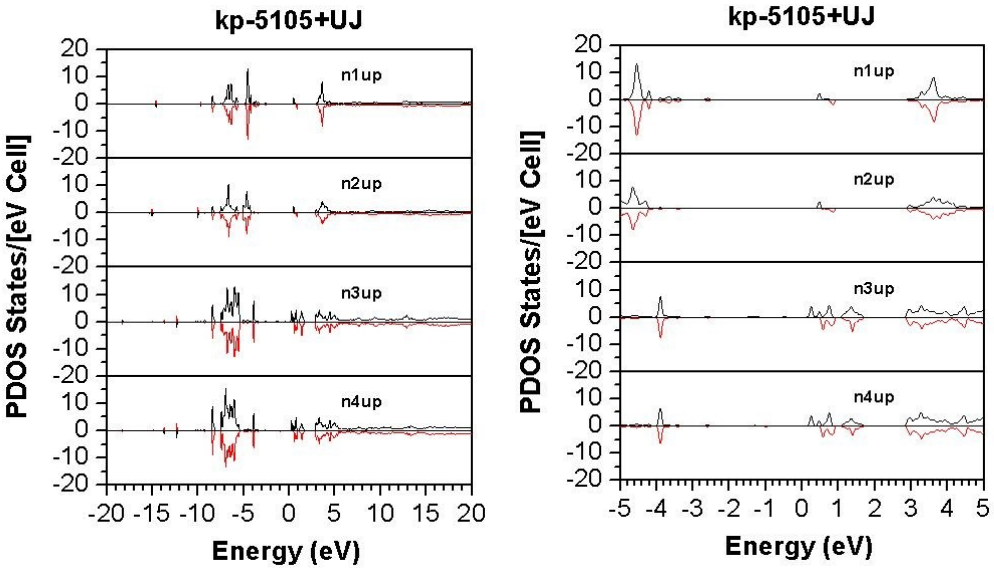

Figure 18: (Left) PDOS for all N types with +UJ. (Right) PDOS for all N types with +UJ in an x range of -5 eV to +5 eV.

Figure 18 shows the PDOS for all N types. Spin splitting is observed for the N types within 2 eV of the Fermi energy, but density of states is low.

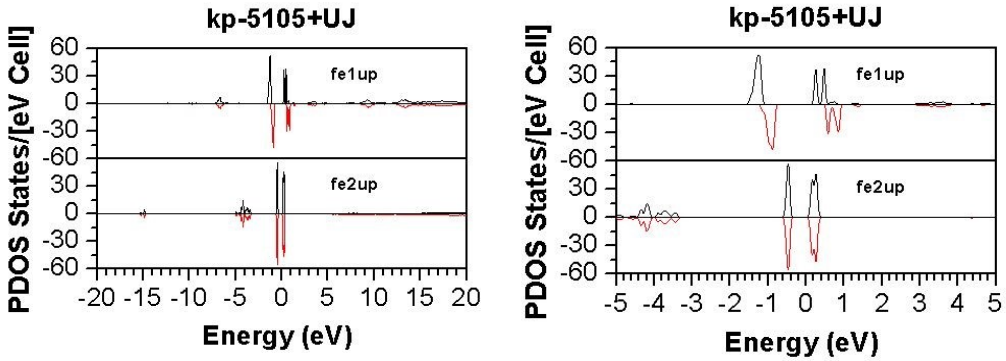

Figure 19: (Left) PDOS for all Fe types with +UJ. (Right) PDOS for all Fe types with +UJ in an x range of -5 eV to +5 eV.

Figure 19 shows a comparison of the PDOS for Fe types 1 and 2; i.e, the Fe^{II} and Fe^{III} species. Again, the most interesting behavior occurs close to the Fermi energy. Spin splitting is apparent for only the Fe^{II} type.

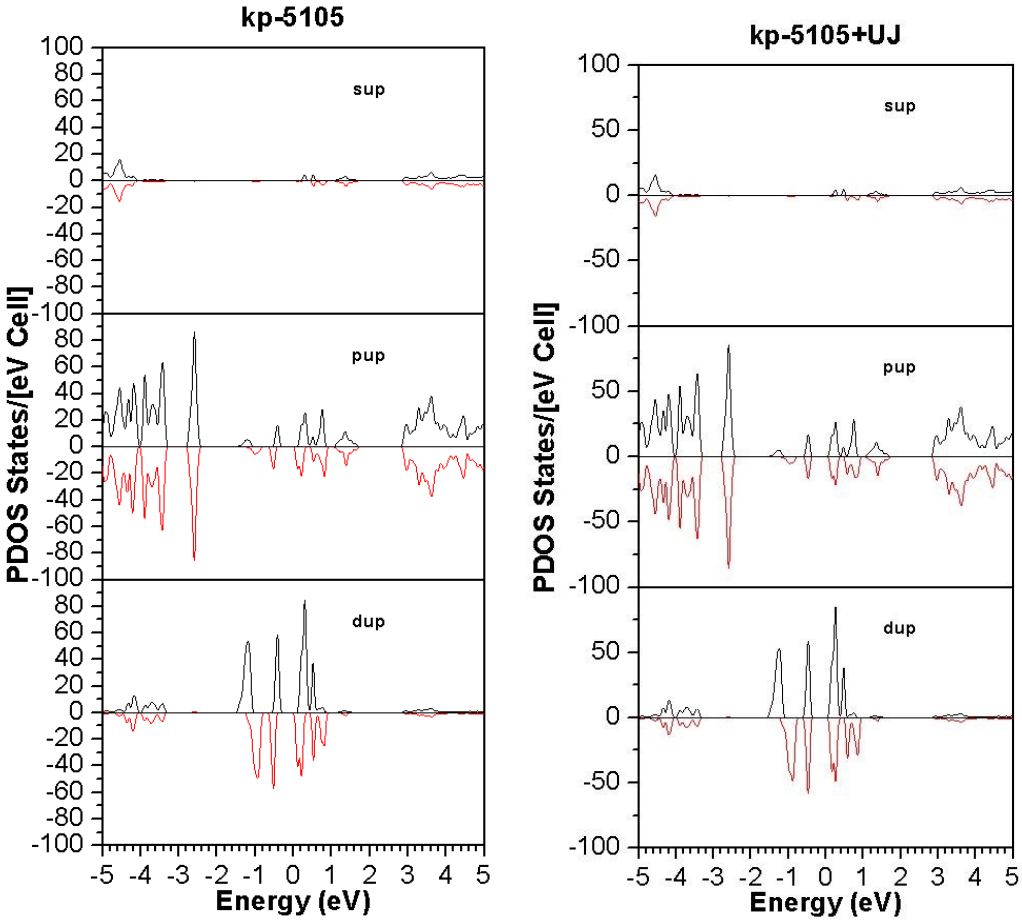

Figure 20: (Left) PDOS for *s*, *p*, and *d* orbitals for all atoms in an x range of -5 eV to +5 eV. (Right) PDOS for *s*, *p*, and *d* orbitals for all atoms with +UJ in an x range of -5 eV to +5 eV.

Figure 20 shows an overall view of the spin up and spin down density of states of *s*, *p*, and *d* orbitals for all atoms before and after the +UJ application. As before, the largest contributors to the density of states are the electrons residing in the *p* and *d* orbitals. Also,

as seen with Fe types 1 and 2 mentioned below, the use of +UJ shifts the spin down peaks slightly to the right for *p* and *d* orbitals.

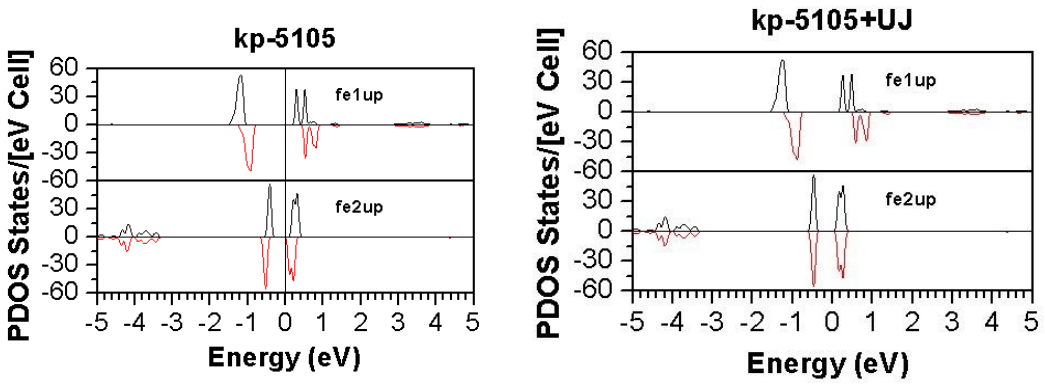

Figure 21: (Left) PDOS for all Fe types in an x range of -5 eV to +5 eV. (Right) PDOS for all Fe types with +UJ in an x range of -5 eV to +5 eV.

Figure 21 shows the PDOS for all Fe types before and after the application of +UJ. There is a clear difference for Fe type 2, Fe^{III}, in regards to spin splitting. The treatment of +UJ shifts the peaks near the Fermi level slightly to the right for both spin up and spin down.

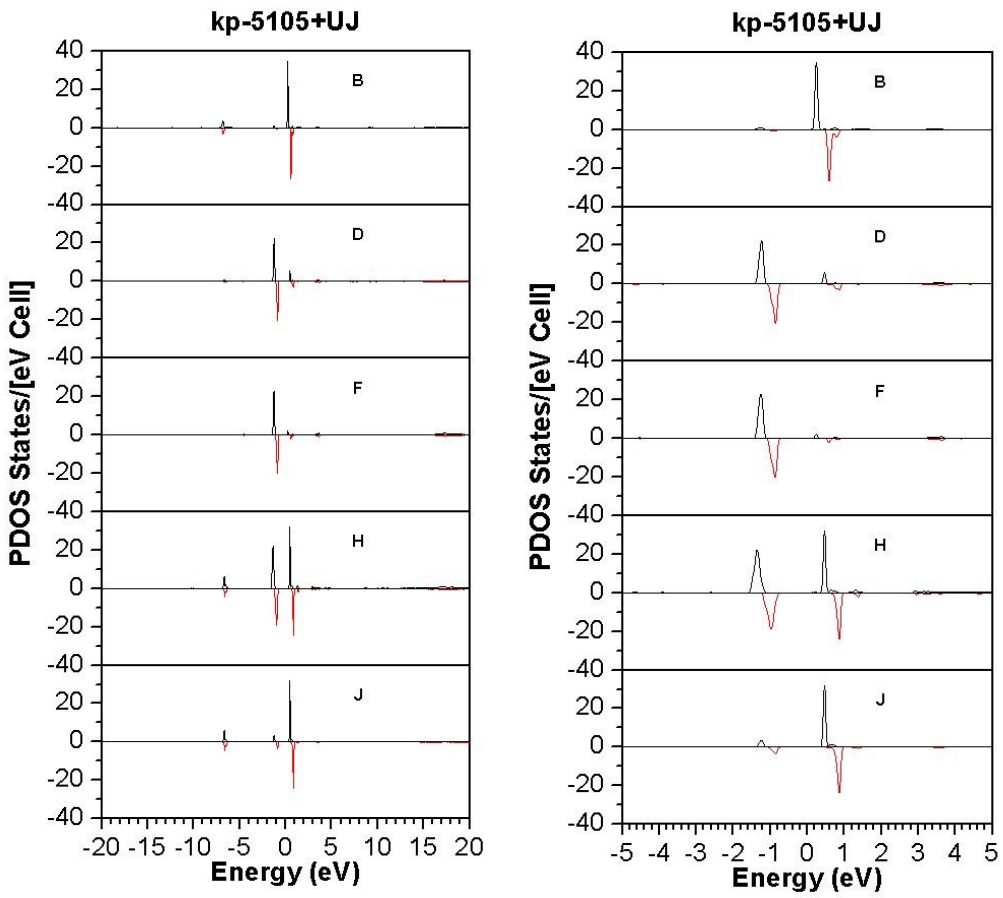

Figure 22: (Left) PDOS for Fe^{II} *d* orbitals. (Right) PDOS for Fe^{II} *d* orbitals in an x range of -5 eV to +5 eV. For both plots, B-J indicates the 5 different *d* orbitals. From top to bottom, *xy*, *xz*, *yz*, x^2-y^2, and dz^2.

Figure 22 shows the PDOS of the Fe^{II} *d* orbitals +UJ. Recall that the Fe^{II} atoms are part of the TCNE layer and thought to add the most to the magnetic ordering. Focusing on the narrow view (Figure 22, Right), the most important *d* orbitals are d_{xy}, $d_{x^2-y^2}$, and d_{z^2}. Contributions from orbitals d_{xz} and d_{yz} are minimal. Spin splitting is evident for all orbitals.

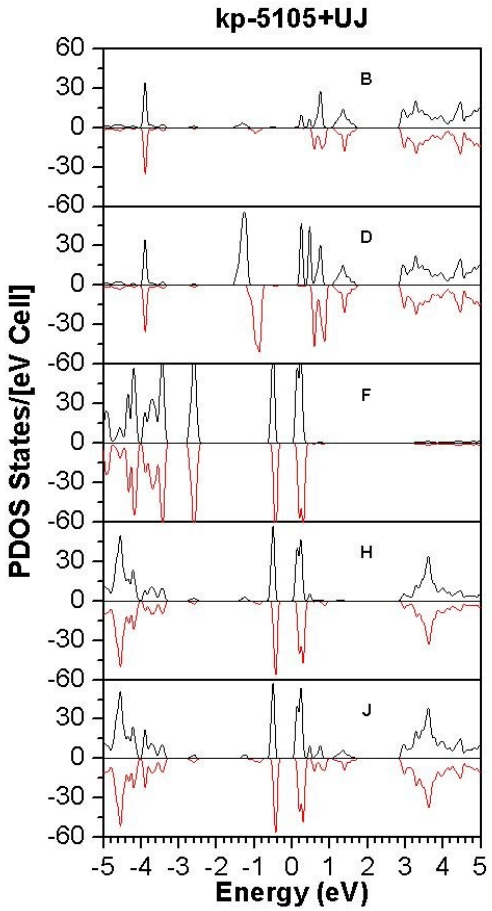

Figure 23: PDOS for various sections of the Fe-TCNE structure with +UJ. For B-J (top to bottom) TCNE, TCNE and the Fe^{II} ion, Cl atoms and Fe^{III} ion, NCMe ligands, and NCMe ligands with Fe^{II} ions.

Figure 23 shows the PDOS for various sections of Fe-TCNE with +UJ; specifically, TCNE itself, TCNE and Fe^{II}, Cl atoms and Fe^{III}, the NCMe ligands, and the NCMe ligands with Fe^{II} atoms. The TCNE and TCNE with Fe^{II} show spin splitting near the Fermi edge. As would be expected with the TCNE/Fe^{II} fragment, the Fe^{II} atoms increase the spin up and spin down density of states values. The Cl/Fe^{III} portion show spin splitting near the

Fermi level. The NCMe and NCMe/Fe^{II} ligands are very similar; the only difference being some extra states between approximately 0.5 eV and 2.0 eV because of Fe^{II}.

Total Density of States with +UJ Application

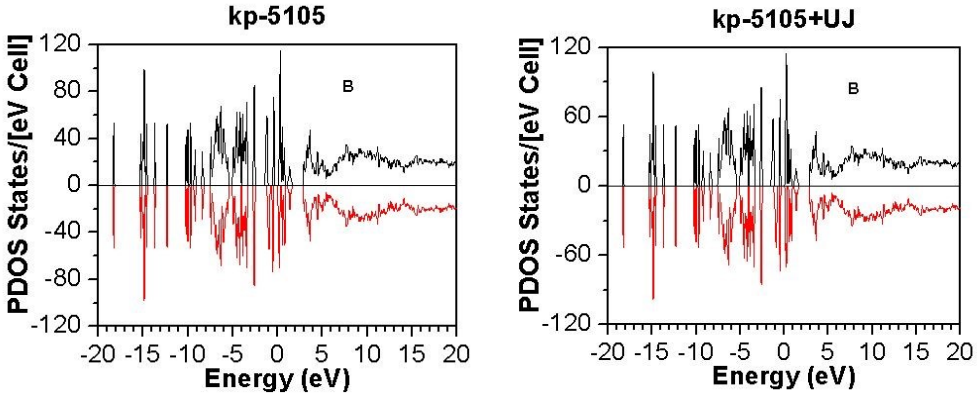

Figure 24: (Left) Total DOS. (Right) Total DOS with +UJ.

Figure 24 shows the Total DOS plots before and after the +UJ treatment. In order to make any comments on these plots a magnified view is needed; this is mentioned below.

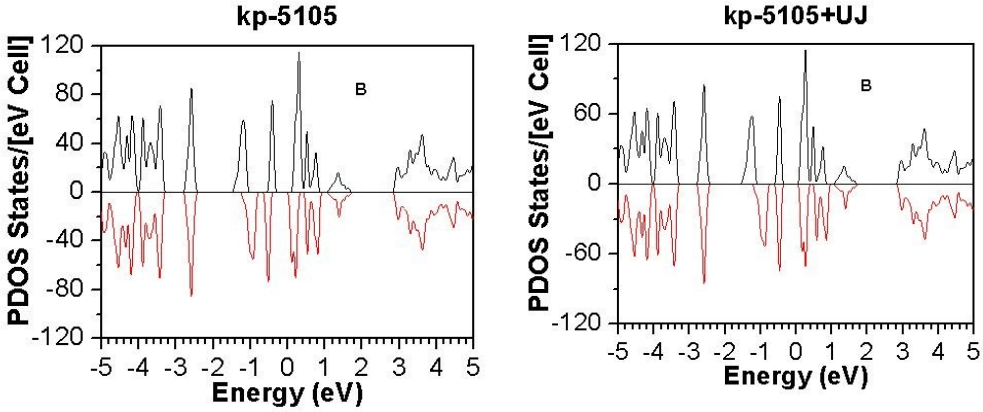

Figure 25: (Left) Total DOS with an x range of -5 eV to +5 eV. (Right) Total DOS with +UJ with an x range of -5 eV to +5 eV.

Figure 25 shows the Total DOS before and after the +UJ application with an x range of -5 eV to +5 eV. The results are consistent with the PDOS and the Fe types plots presented earlier; i.e., the spin down peaks shift slightly to the right.

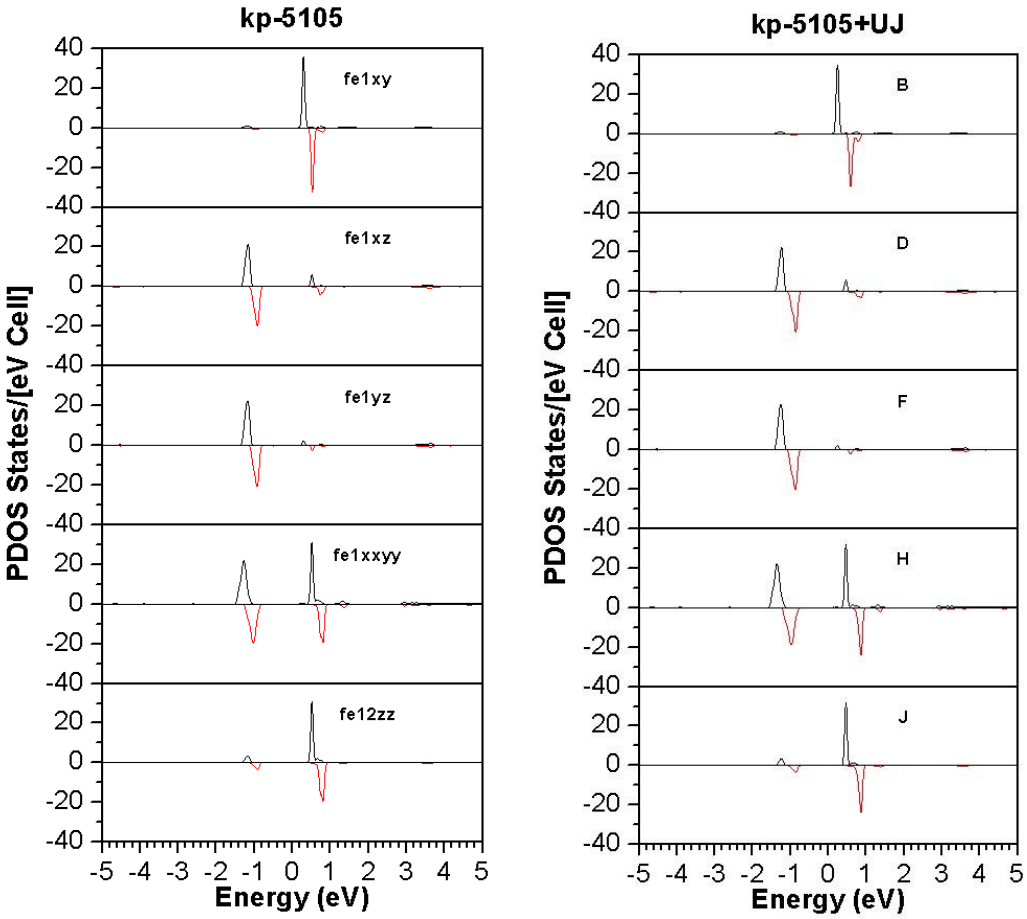

Figure 26: (Left) PDOS for Fe^{II} *d* orbtials in an x range of -5 eV to +5 eV. (Right) PDOS for Fe^{II} *d* orbitals in an x range of -5 eV to +5 eV. B-J indicates the 5 different *d* orbitals. From top to bottom, *xy*, *xz*, *yz*, x^2-y^2, and dz^2.

Figure 26 shows the PDOS for the Fe^{II} *d* orbitals before and after the application of +UJ. The treatment of +UJ shifts the peaks near the Fermi level slightly to the right for spin down peaks for all *d* orbitals.

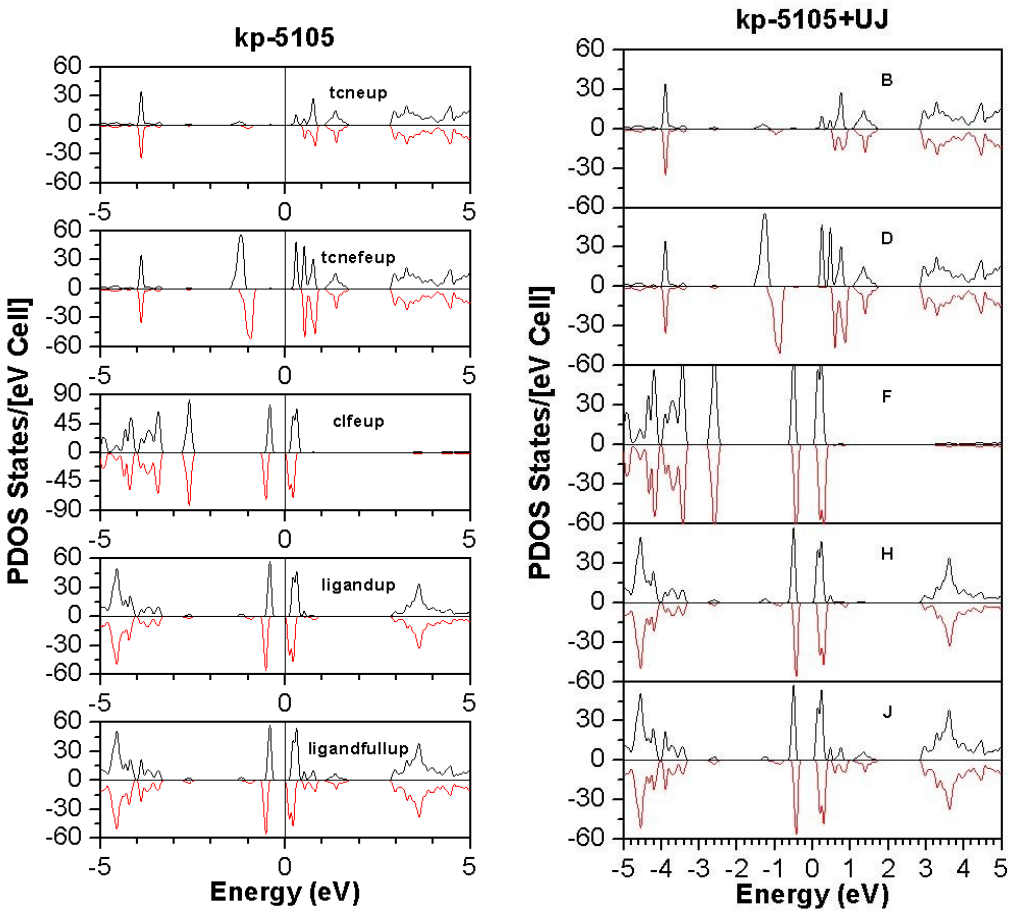

Figure 27: (Left) PDOS for various sections of the Fe-TCNE structure. From top to bottom, TCNE, TCNE and the Fe^{II} ion, Cl atoms and Fe^{III} ion, NCMe ligands, and NCMe ligands with Fe^{II} ions. (Right) PDOS for various sections of the Fe-TCNE structure with +UJ. For B-J (top to bottom) TCNE, TCNE and the Fe^{II} ion, Cl atoms and Fe^{III} ion, NCMe ligands, and NCMe ligands with Fe^{II} ions.

Figure 27 shows the PDOS for various sections of Fe-TCNE before and after +UJ; specifically, TCNE itself, TCNE and Fe^{II}, Cl atoms and Fe^{III}, the NCMe ligands, and the NCMe ligands with Fe^{II} atoms. The TCNE and TCNE with Fe^{II} show spin splitting near the Fermi edge. Again, as is expected with the TCNE/Fe^{II} fragment, the Fe^{II} atoms increase

the spin up and spin down density of states values. The Cl/Fe^{III} portion show spin splitting near the Fermi level. The NCMe and $NCMe/Fe^{II}$ ligands are very similar; the only difference being some extra states between approximately 0.5 eV and 2.0 eV because of Fe^{II}. As previously seen in comparisons between prior to and after the +UJ application, the spin down density of states peaks near the Fermi energy level shift slightly to the right.

CHAPTER 5
CONCLUSIONS AND FUTURE WORK

Conclusions

The work in this thesis sought to apply the LSDA+U method to a specific organic-based magnet material within the general TCNE family of materials and to incorporate the +UJ potential into the overall structure of the OLCAO program suite. The second objective will be reviewed first.

The LSDA+U formalism and the incorporation of the Anisimov potential have been successfully integrated into OLCAO, including for both *d* and *f* orbitals. This addition can now find use in future calculations to better describe the electronic structure and band gap of other Mott insulators and late 3*d*-transition metal materials. The implementation of the +U formalism can better elucidate the electronic structure and magnetic ordering for magnetic materials as well.

The application of the +UJ potential to Fe-TCNE was performed and differences were noted for the overall *p* and *d* orbitals, the Fe types, and the Fe type 1, Fe^{II}, *d* orbitals. Although the +UJ treatment was expected to yield a more significant increase in the band gap than what was observed, the results are still a better description of the on-site Coulombic repulsion than what was available before. The band gap increased from 0.04 eV to 1.2 eV. In addition, the shifting of the density of states peaks led to a better account of the spin splitting that leads to magnetism; specifically, the spin up and spin down peaks that included Fe^{II} atoms were separated by a greater amount.

Future Work

A number of interesting activities could be performed as an extension of the work in this thesis. First, performing calculations to look at the optical properties would be interesting, in addition to XANES and ELNES calculations. Second, exploring the parameter space of different U and J values for Fe type 1, as well as different values for other atom types, could prove to yield a better description of the electronic structure. Finally, considering U and J values obtained from a first principles method, like constrained DFT, could reduce the time needed to explore the parameter space. A likely candidate for those would be using Slater integrals, F^k.

REFERENCES

[1] J. Hafner, C. Wolverton, and G. Ceder, MRS Bull. **31**, 659 (2006).
[2] P. Biswas, D. N. Tafen, F. Inam, B. Cai, and D. A. Drabold, J Phys Condens Matter **21**, 1 (2009).
[3] J. S. Miller and A. J. Epstein, Angew Chem Int Ed Engl **33**, 385 (1994).
[4] J. S. Miller, Mater. Today **17**, 224 (2014).
[5] C. P. Landee, D. Melville, and J. S. Miller, *Magn. Mol. Mater.* (1991), pp. 395–398.
[6] National Science and Technology Council, *Materials Genome Initiative for Global Competitiveness*, (https://www.mgi.gov/sites/default/files/documents/materials_genome_initiative-final.pdf) (2011).
[7] Department of Energy Workshop, *Computational Materials Science and Chemistry for Innonvation*, (https://science.energy.gov/~/media/bes/pdf/reports/files/Computational_Materials_Science_and_Chemistry_rpt.pdf) (United States Department of Energy, 2010).
[8] R. Hasegawa, J. Non-Cryst. Solids **287**, 405 (2001).
[9] A. Inoue and N. Nishiyama, MRS Bull. **32**, 651 (2007).
[10] R. Hasegawa, J. Magn. Magn. Mater. **100**, 1 (1991).
[11] R. Hasegawa, J. Magn. Magn. Mater. **215-216**, 240 (2000).
[12] J. S. Miller, Dalton Trans. 2742 (2006).
[13] P. Hohenberg and W. Kohn, Phys. Rev. **136**, B864 (1964).
[14] W. Kohn and L.J. Sham, Phys. Rev. **140**, A1133 (1965).
[15] K. I. Pokhodnya, M. Bonner, J.-H. Her, P. W. Stephens, and J. S. Miller, J Am Chem Soc **128**, 15592 (2006).
[16] J.-W. Yoo, V. N. Prigodin, W. W. Shum, K. I. Pokhodnya, J. S. Miller, and A. J. Epstein, Phys. Rev. Lett. **101**, 197206 (2008).
[17] A. N. Caruso, K. I. Pokhodnya, W. W. Shum, W. Y. Ching, B. Anderson, M. T. Bremer, E. Vescovo, P. Rulis, A. J. Epstein, and J. S. Miller, Phys. Rev. B **79**, 195202 (2009).
[18] W. W. Shum, A. J. Epstein, and J. S. Miller, Phys. Rev. B **80**, 064403 (2009).
[19] M. Born and R. Oppenheimer, Ann. Phys. **389**, 457 (1927).
[20] D. Hartree, Math. Proc. Camb. Philos. Soc. **24**, 89 (1928).
[21] V. Fock, Z. Phys. **61**, 126 (1930).
[22] P.-O. Lowdin, Adv. Chem. Phys. **2**, 207 (1959).
[23] G.H. Booth, A. Grüneis, G. Kresse, and A. Alavi, Nature **493**, 365 (2012).
[24] C.D. Sherrill and H.F. Schaefer III, Adv. Quantum Chem. **34**, 143 (1999).
[25] C. Moller and M.S. Plesset, Phys. Rev. **46**, 618 (1934).
[26] J. Cizek, J. Chem. Phys. **45**, 4256 (1966).
[27] J. Cizek and J. Paldus, Int. J. Quantum Chem. **5**, 359 (1971).
[28] R.G. Parr, Annu. Rev. Phys. Chem. **34**, 631 (1983).
[29] T. Ziegler, Chem. Rev. **91**, 651 (1991).
[30] P. Geerlings, F. De Proft, and W. Langenaeker, Chem. Rev. **103**, 1793 (2003).
[31] R.O. Jones and O. Gunnarsson, Rev. Mod. Phys. **61**, 689 (1989).
[32] R.G. Parr and W. Yang, *Density-Functional Theory of Atoms and Molecules* (Oxford University Press, New York, 1989).

[33] M.R. Dreizler and E.K.U. Gross, *Density Functional Theory: An Approach to the Quantum Many-Body Problem* (Springer, Berlin, 1990).
[34] L.H. Thomas, Math. Proc. Camb. Philos. Soc. **23**, 542 (1927).
[35] E. Fermi, Rend Accad Naz Lincei **6**, 602 (1927).
[36] A.D. Becke, J. Chem. Phys. **88**, 1053 (1988).
[37] J.P. Perdew and K. Schmidt, in (AIP Conference Proceedings, 2001), (http://dft.uci.edu/pubs/PB96.pdf), pp. 1–20.
[38] L. Hedin and B.I. Lundqvist, J. Phys. C Solid State Phys. **4**, 2064 (1971).
[39] D.M. Ceperley and B.J. Alder, Phys. Rev. Lett. **45**, (1980).
[40] S.H. Vosko, L. Wilk, and M. Nusair, Can. J. Phys. **58**, 1200 (1980).
[41] J.P. Perdew and A. Zunger, Phys. Rev. B **23**, 5048 (1981).
[42] L.A. Cole and J.P. Perdew, Phys. Rev. A **25**, 1265 (1982).
[43] J.P. Perdew and Y. Wang, Phys. Rev. B **45**, 13244 (1992).
[44] J.P. Perdew and K. Burke, Int. J. Quantum Chem. **57**, 309 (1996).
[45] M. Levy and J.P. Perdew, Int. J. Quantum Chem. **49**, 539 (1994).
[46] J. Tao, J.P. Perdew, V.N. Staroverov, and G.E. Scuseria, Phys. Rev. Lett. **91**, (2003).
[47] J. Hubbard, Proc. R. Soc. Lond. Ser. Math. Phys. Sci. **276**, 238 (1963).
[48] J. Hubbard, Proc. R. Soc. Lond. Ser. Math. Phys. Sci. **277**, 237 (1964).
[49] J. Hubbard, Proc. R. Soc. Lond. Ser. Math. Phys. Sci. **281**, 401 (1964).
[50] A. Mielke and H. Tasaki, Commun. Math. Phys. **158**, 341 (1993).
[51] H. Tasaki, Phys. Rev. Lett. **75**, 4678 (1995).
[52] A. Mielke, Phys. Lett. A **174**, 443 (1993).
[53] S. Arya, P.V. Sriluckshmy, S.R. Hassan, and A.-M.S. Tremblay, Phys. Rev. B **92**, 045111 (2015).
[54] K. Kubo and M. Uchinami, Prog. Theor. Phys. **54**, 1289 (1975).
[55] J. Kaczmarczyk, J. Spalek, T. Schickling, and J. Bunemann, Phys. Rev. B **88**, 115127 (2013).
[56] T.A. Maier, J.B. White, M. Jarrell, P. Kent, and T.C. Schulthess, J. Phys. Conf. Ser. **16**, 257 (2005).
[57] H.T. Dang, X.Y. Xu, K.-S. Chen, Z.Y. Meng, and S. Wessel, Phys. Rev. B **91**, 155101 (2015).
[58] A. Yamada, Phys. Rev. B **89**, 195108 (2014).
[59] V. Anisimov, J. Zaanen, and O. Andersen, Phys. Rev. B **44**, 943 (1991).
[60] A.I. Liechtenstein, V.I. Anisimov, and J. Zaanen, Phys. Rev. B **52**, R5467 (1995).
[61] M.J. Han, T. Ozaki, and J. Yu, Phys. Rev. B **73**, (2006).
[62] W.-Y. Ching and P. Rulis, *Electronic Structure Methods for Complex Methods: The Orthogonalized Linear Combination of Atomic Orbitals*, 1st ed. (Oxford University Press, 2012).

VITA

Steven Chase Grafton was born on October 28, 1983 in Kansas City, Missouri. He attended the Blue Springs school district completing his high school education in 2002 from Blue Springs South High School. He graduated with a Bachelor of Science in Physics from the University of Missouri – Columbia in 2006.

He has been employed as an engineer with the National Nuclear Security Administration's Kansas City National Security Campus, contractor to Honeywell Federal Manufacturing & Technologies, since 2007.

He is a member of the American Physical Society (APS).